Sonic Boom Computations for a Mach 1.6 Cruise Low Boom Configuration and Comparisons with Wind Tunnel Data

Alaa A. Elmiligui[1]
Floyd Wilcox[3]
Linda Bangert[5]

NASA Langley Research Center
Hampton, VA, 23681

Susan E. Cliff[2]
Marian Nemec[4]
Michael J. Aftosmis[6]

NASA Ames Research Center
Moffett Field, CA 94035

Edward Parlette[7]
ViGYAN, Inc., Hampton, VA 23666

Accurate analysis of sonic boom pressure signatures using computational-fluid-dynamics techniques remains quite challenging. Although CFD shows accurate predictions of flow around complex configurations, generating grids that can resolve the sonic boom signature far away from the aircraft is a challenge. The test case chosen for this study corresponds to an experimental wind-tunnel test that was conducted to measure the sonic boom pressure signature of a low boom configuration designed by Gulfstream Aerospace Corporation. Two widely used NASA codes, USM3D and AERO, are examined to determine their ability to accurately capture sonic boom signature. Numerical simulations are conducted for a free-stream Mach number of 1.6, angle of attack of 0.3 and Reynolds number of 3.85x10^6 based on model reference length. Flow around the low boom configuration in free air and inside the NASA Langley Unitary Plan Wind Tunnel are computed. Results from the numerical simulations are compared with wind tunnel data. The effects of viscous and turbulence modeling along with tunnel walls on the computed sonic boom signature are presented and discussed.

Nomenclature

CATIA	=	Computer Aided Three-dimensional Interactive Application
C_p	=	pressure coefficient
DELX	=	distance between model nose and centerline survey probe orifice
DP / P	=	overpressure coefficient = $(P - P_\infty) / P_\infty$ in free air; $(P - P_r)/P_r$ in tunnel
h, H	=	altitude or distance from model
l, L	=	reference model length, 13.2 in
LBC	=	low boom configuration

[1] Research Aerospace Engineer, Configuration Aerodynamics Branch, M/S 499-1, Hampton, VA 23681, AIAA Senior Member
[2] Aerospace Engineer, NAS Applications Branch, M/S 258-2, Moffett Field, CA 94035, AIAA Associate Fellow
[3] Aerospace Engineer, Configuration Aerodynamics Branch, M/S 499-1, Hampton, VA 23681.
[4] Senior Research Scientist, Science & Technology Corp., Applied Modeling and Simulation Branch, MS 258-5, Moffett Field, CA 94035, AIAA Senior Member
[5] Aerospace Engineer, Configuration Aerodynamics Branch, , M/S 499-1, Hampton, VA 23681, AIAA Associate Fellow
[6] Aerospace Engineer, Applied Modeling and Simulation Branch, MS 258-5, Moffett Field, CA 94035, AIAA Associate Fellow
[7] Research Engineer, VIGYAN Research Associates, 30 Research Dr., MS 130, Hampton, VA 23666

P	=	static pressure
P_∞	=	freestream static pressure
P_r	=	tunnel reference pressure
Re_L	=	Reynolds number based on the model reference length L
UPWT	=	NASA Langley Unitary Plan Wind Tunnel
WTT	=	wind tunnel test
X	=	axial axis
Xnose	=	model nose axial location
Y	=	spanwise axis
Z	=	vertical axis
α	=	angle of attack
φ	=	off track angle
ϑ_v	=	vertical flow angle
ϑ_H	=	horizontal flow angle
μ	=	Mach angle
ν	=	shearing angle

I. Introduction

A wind-tunnel test (WTT) was conducted to measure the sonic boom pressure signature of a low boom configuration (LBC) designed by Gulfstream Aerospace Corporation (GAC). The WTT was a joint cooperation between GAC and the National Aeronautics and Space Administration (NASA) Langley Research Center (LaRC)[1,1]. The WTT was conducted in the NASA Langley Unitary Plan Wind Tunnel (UPWT) at free-stream Mach numbers of 1.6 and 1.8. The Reynolds number (Re_L), at both Mach numbers, was $3.85\text{x}10^6$ based on the model reference length. Sonic-boom pressure signatures were measured at distances ranging from 0.5 to 1.7 body lengths. On- and off-track sonic-boom pressure signatures, surface pressures, model normal force and pitching moment were acquired. The test was conducted as part of the Supersonic Cruise Efficiency – Airframe element of the NASA Fundamental Aeronautics Program Supersonics Project. The objective of the Supersonic Cruise Efficiency element is to improve aerodynamic design and analysis capability for highly efficient, supersonic vehicles. The primary technical challenge of the Supersonic Cruise Efficiency element is to develop robust CFD-based methods for rapid design and analysis of supersonic cruise aircraft that are highly efficient, and have low sonic boom. The test was divided into two parts. In the first part, GAC conducted a WTT to measure the sonic boom signature on a LBC. At the end of the test, after all sonic boom measurements were completed, flow Schlieren images were acquired. In the second part of the test, NASA conducted a brief flow visualization study to determine the effect of boundary layer transition grit on the measured sonic boom signature of the LBC. A follow up WTT was also conducted at NASA Ames research center to measure the sonic boom signature of the LBC[1] .

Computational fluid dynamics (CFD) analysis was also conducted on the LBC[1-1]. Comparison of the computed low boom signature to WTT data showed good agreement for the forward part of the signature, but less favorable agreement for the aft part of the signature. CFD analysis of the sonic boom pressure signatures remains quite challenging[1-1]. Specialized grids that place grid points within the zone of influence of the sonic boom disturbance or solution-adaptive methods are typically applied to obtain accurate solutions. The authors have recently evaluated methods that use domain rotation of Cartesian grids, developed knowledge-based grid refinement EASS (Elliptical/Annular Swept Sector) techniques for tetrahedral meshes[1], tetrahedral-based grid methods that employs projected Mach cone aligned prism cells (MCAP)[1], and stretching and shearing methods[1] (SSGRID methodology) from seeded tetrahedral grids.

In the present paper, the effects of viscous and turbulence modeling along with the tunnel wall effects on the computed sonic boom signature are evaluated. The flow around the LBC in free air as well as in NASA Langley UPWT is computed and compared to wind tunnel data. Numerical simulations are conducted for a free-stream Mach number of 1.6, angle of attack of 0.3, H/L = 1.7, and Reynolds number of $3.85\text{x}10^6$. The CFD codes used in the study were the Unstructured Mesh Three Dimensional (USM3D)[1-1] solver and the Adjoint Error Optimization system (AERO)[1-1]. USM3D is a tetrahedral cell-centered, finite volume Euler and Navier-Stokes (N-S) flow solver that was used to provide inviscid, laminar and turbulent flow simulations of the LBC in free air. AERO extends the capabilities of NASA's inviscid, embedded-boundary Cartesian mesh solver, Cart3D, to include adjoint-based error estimation and automatic mesh refinement. AERO has been verified and validated over a broad range of problems, including supersonic performance and low-boom studies.[1] AERO provided solutions for the LBC model inside the NASA Langley 4X4 UPWT as well as in free air. The results of this study will help address the issue of tunnel effects and viscous modeling on the measured supersonic boom signature. Comparison of the computed low boom signature and measured wind tunnel data will be presented and discussed.

The organization of this paper is as follows: (1) a brief description of the wind tunnel test and data reduction (2) descriptions of the CFD codes, USM3D and AERO, used in the study, (3) presentation of the numerical results along with discussion and comparison to wind tunnel data and (4) concluding remarks.

II. Unitary Plan Wind Tunnel Test

A. Unitary Plan Wind Tunnel (UPWT)

The wind tunnel test was conducted in the low Mach number test section of the NASA Langley UPWT, which is a continuous flow, variable pressure, supersonic wind tunnel with two test sections. A complete description of the facility along with test section calibration information is contained in reference 1. The test section is approximately 4 ft square and 7 ft long. The nozzle leading to the test section has an asymmetric sliding block, which permits continuous variation of Mach number from 1.50 to 2.90 in the low Mach number test section (test section 1). The WTT was conducted at Mach numbers of 1.6 and 1.8 and at a Reynolds number of 3.85×10^6. Figure 1 shows a photograph of the model mounted in the test section. In the present paper, the flow inside the nozzle and test section 1 was computed and compared to WTT data at a Mach of 1.6 and a Reynolds number of 3.85×10^6.

B. Low Boom Model And Pressure Measuring Probes

A schematic of the low boom configuration model designed by GAC is shown in Fig. 2. The low boom model reference length, chord, span, and area are 13.2 in., 2.1029 in., 4.3594 in., and 8.64 in.^{2} respectively. A telescoping nose is a key identifying feature of the LBC. It was designed to replace a single nose shock with small controlled pressure oscillations to reduce the sonic boom loudness level. The model is mounted on a blade shaped sting designed by GAC. The sting attachs to the upper surface of the model to minimize interference with the sonic boom signature below the configuration.[1] The top mounted sting is a state-of-the-art approach that permits accurate measurements of the empennage flow field. This mounting system was designed to simulate flight and was carefully designed to have minimal on the pressure signature.

The low boom signature was measured with four static pressure probes mounted on the west tunnel wall door blank. Figure 3 shows top and side views of reference and survey probes as mounted in the UPWT. One probe served as a reference probe and measured the free stream static pressure and remained in a fixed position. All three survey probes were in the same vertical plane and were mounted on an axial traverse mechanism. The relative distance between all four probes and their relative location in the tunnel is shown in Fig. 3. The survey probes were mounted on a traverse so that the probes can be moved longitudinally in the tunnel. Figure 4 shows a photograph of the traversing mechanism and survey probes mounted in the tunnel. The reference probe pressure was used as the reference for all of the survey probes.

C. Wind Tunnel Test Procedure and Data Reduction

A typical sonic boom pressure signature WTT run consisted of first adjusting the angle of attack mechanism so that a given normal force was obtained on the model. Using the tunnel model support system, the model is laterally positioned at a specified distance, h, from the on-track (centerline) survey probe. Initially, the model was located so that the bow shock is downstream of the survey probes. The model is moved forward in 0.125 in. increments over the survey probes to obtain the pressure signature data from the reference and survey static pressure probes. As the model is moved forward the normal force coefficient varies primarily because of stream angle variations and flow field pressure gradients within the test section. Data is acquired in a move/pause mode of operation. For each pressure signature, the model was moved approximately 24 inches.

On- and off-track sonic-boom pressure signatures, surface pressures, model normal force and pitching moment were measured at distances that ranged from 0.5 to 1.7 body length for a range of Mach numbers from 1.6 to 1.8, for three angles of attack (-0.25°, 0.25°, 0.69°). The tunnel air dew point was maintained below -20°F (at atmospheric pressure) to minimize water vapor condensation. Maintaining a low humidity level is very important in sonic boom wind tunnel testing. Further details of the tunnel running conditions, the effects of Mach number, H/L, angle of attack, survey probe position, and boundary layer transition grit on the sonic boom signature are presented in references 1 and 2.

Figure 5 shows good long-term data repeatability. The very small pressure oscillations from the segmented nose have better repeatability than the larger shocks in the aft portion of the pressure signatures Figure 5 illustrates the salient features of the low boom signature data; the pressure peaks from the nose tip and the four nose segments are clearly visible in the plot. Figure 6 shows three sequential sonic boom signature runs that differ by 2 inches in the position of the survey probes (remotely controlled translation). Ideally, these runs should be as repeatable as the repeat runs shown in Fig. 5. However, the results indicate that there is additional scatter in the data. The variation in tunnel flow conditions as a function of location within the test section is the factor in the additional data scatter.

During the WTT, sublimation tests were conducted to determine the size and location of boundary layer grit that would transition the boundary layer flow from laminar to turbulent. The transition strips consisted of sand grit sparsely sprinkled in a lacquer film and are shown in Fig. 7. The effect of boundary layer grit on the sonic boom signatures for M = 1.60 is shown in Fig. 8. The primary affect of the boundary layer grit is seen downstream of the wing expansion. Turbulent flow over the model wing does not significantly affect the peak pressures generated by the wing. The grit located on the model nose does not create a noticeable pressure peak, whereas, the wing boundary layer grit does show a compression, expansion, and re-compression at DELX $\approx$ 32 in.

III. General Description of Computational Methods

The two NASA software systems used for the computational analysis were the Tetrahedral Unstructured Software System (TetrUSS)[1] and AERO[1] package. GAC delivered the as built surface definition of LBC in CATIA part format. NASA LaRC Geometry Laboratory used the CATIA files to prepare and deliver the as-built surface definition in a PLOT3D unformatted, double precision file format. The as-design sting surface definition was then added to LBC. TetrUSS and AERO used the same surface mesh. The computational grids, flow solvers, and the boundary conditions for USM3D and AERO are described below.

A. Tetrahedral Unstructured Software System (TetrUSS)

TetrUSS was developed at NASA Langley Research Center and includes; a model/surface grid preparation tool (GridTool), field grid generation software (VGRID, POSTGRID) and a computational flow solver (USM3D). The USM3D flow solver has internal software to calculate forces and moments. Additionally, the NASA LaRC-developed code USMC6[1] was used for analyzing the solutions.

TetrUSS Computational Grids

For the LBC in free air, inviscid and viscous volume grids were generated by the Mach Cone Aligned Prism (MCAP) approach[1]. A refined unstructured grid within a cylinder in the near field is followed by projection of the surface faces on the cylindrical boundary in the radial direction with a series of prism layers to the far field. The MCAP method maintains highly refined grid spacing in the axial direction throughout the entire mesh, and allows control of the radial stretching and shearing (to align with the Mach cone angle around the aircraft). Projecting each triangular face forms a prism that is then sheared to align with the Mach angle. More details about MCAP method can be found in reference 1. The inviscid grid consisted of 72 million cells while the viscous grid had 130 million cells. Figure 9 shows a planar cut showing the USM3D grid distribution for the viscous grid. Some guidelines for grid generation included the requirement for surface cell size to be small enough to resolve features and curvature of the LBC. Proper boundary layer spacing was used to ensure y+ remains less than or equal to 1 for the selected free stream Mach and Reynolds numbers. It is beneficial to start aligning the mesh as close to the body as possible for accurate sonic boom pressure signatures even at distances less than one body length.

Surface patches were created on the configuration in GridTool[1] using a PLOT3D surface definition of the geometry. Sources were placed throughout the domain to cluster cells and accurately capture configuration characteristics. The output from GridTool was used to automatically generate the computational domain with the VGRID unstructured grid generation software. VGRID uses an Advancing Layers Method to generate thin layers of unstructured tetrahedral cells in the viscous boundary layer,[1] and an Advancing Front Method to populate the volume mesh in an orderly fashion.[1] POSTGRID was used to close the grid by filling in any gaps that remain from VGRID. POSTGRID is automated to carefully remove a few cells surrounding any gaps in the grid and precisely fill the cavity with the required tetrahedral cells. The generated volume grids, modeling the tunnel interior, failed to resolve sonic boom signatures. The authors are currently working on refining this process of grid generation to be able to capture sonic boom in a computational mesh that models the inside of a wind tunnel. Figure 10 shows schematic of LBC inside the UPWT.

TetrUSS FlowSolver USM3D

The flow solver for the TetrUSS software package is USM3D. USM3D is a tetrahedral cell-centered, finite volume Euler and Navier-Stokes (N-S) method. The USM3D flow solver has a variety of options for solving the flow equations and several turbulence models for closure of the N-S equations.[1-1] A script program, written as part of the Ares V project guidelines development, was used to automatically setup input parameters for choosing the proper flux scheme and CFL numbers based on the desired Mach number for each case.[28] For the current study, Roe's flux difference splitting scheme was used and CFLmax was set to 20. Flux limiters are used within CFD codes to preclude oscillations due to shocks and discontinuities by limiting the values of the spatial derivatives. Typically, a flux limiter is required for supersonic flows and not for subsonic flow computations. For the present study, at the start of a new solution, the USM3D code ran 10000 iterations with first order spatial accuracy, and then the code automatically switched to second order spatial accuracy. Figure 11 shows convergence history for the LBC in free air using the Menter shear stress transport (SST) turbulence model. Details of the implementation of the SST turbulence model within USM3D can be found in reference 1.

B. AERO Package

The AERO package computes a reliable approximation of user-selected outputs, such as pressure signatures, through the use of adjoint error estimation and automatic mesh refinement. It allows users to perform automated CFD analysis of complex geometries and is particularly effective in preliminary aerodynamic design.

AERO Computational Grids

The computational mesh consists of regular hexahedra everywhere, except for a layer of body-intersecting cells, or cut-cells, adjacent to the boundaries. AERO uses adjoint-weighted residual error-estimates to guide automatic mesh adaptation. Once a user specifies outputs of interest (lift, drag, etc.) with a corresponding error tolerance, AERO automatically refines meshes to drive the remaining numerical errors in the outputs below the requested tolerance.[25] In the current study, the goal was the evaluation of the sonic boom pressure signature. Hence, the functional of interest was selected as a pressure coefficient 'sensor' along a line in the domain given by:

$$J = \int_0^l \left(\frac{DP}{P}\right)^2 ds$$

Computations of model-in-tunnel cases involved two co-linear, equally weighted line sensors at 1.7 body lengths below the model. The second line sensor was used to emphasize the nose spike shocks and provide a solution with less mesh points.

AERO Flow Solver

A multilevel flow solver is used for all computations with domain-decomposition to achieve very good scalability[1]. The spatial discretization uses a cell-centred, second-order accurate finite volume method with a weak imposition of boundary conditions. The flux-vector splitting approach of van Leer is used in conjunction with the Barth-Jespersen limiter. Convergence to steady-state is obtained via a five stage Runge-Kutta scheme and multigrid. Further details are given in references.[1-1]

C. Initial and Boundary Conditions

For the inviscid flow simulations, an inviscid aerodynamic surface boundary condition (BC) was used on all solid surfaces. The supersonic inflow BC was used at the domain inflow face and the extrapolation BC was used at the downstream outflow face of the domain. The characteristic inflow and outflow BC was used along the far field, lateral faces of the outer domain. For USM3D viscous simulation the no-slip viscous BC was used on all solid surfaces of the LBC. For the model-in-tunnel simulations, AERO utilized a prescribed surface BC at the inlet and exit surfaces, while USM3D used the jet BC at the inlet boundary and full extrapolation, supersonic outflow BC at the exit.

IV. Results

The flow field around the LBC was computed using TetrUSS and AERO for a free-stream Mach number of 1.6, $\alpha = 0.3°$ to match WTT force coefficients, and a Reynolds number of $3.85\text{x}10^6$. The computational results of the LBC in free air will be presented first, followed by computations of the internal flow of the UPWT, "empty tunnel", and lastly, the LBC in the UPWT. The LBC in the UPWT was evaluated at four axial locations, at Xnose of -5, 0, 5, and 10 inches. A summary of all meshes generated by AERO is shown in Table 1. The free-air case uses approximately 10 million cells, while the model-in-tunnel cases used over a 100 million cells. All computations were started from coarse meshes involving just 20,000 cells.

Table 1. Cell Count For The Various Grids used in AERO Calculations.

Case	Initial Mesh cell Count	Final Mesh cell count	Adaption Level
Model in Free Air	21,000	9,889,164	11
Empty Tunnel	20,857	113,708,596	13
Model @ x = -5	20,857	111,678,140	13
Model @ x = 0	20,857	106,120,140	13
Model @ x = 5	20,856	116,158401	13
Model @ x = 10	20,856	116,26,6040	13

A. LBC in Free Air

Figure 12 shows the symmetry plane of the AERO grid colored with Cp for LBC in free air. The grid has about ten million cells after eleven levels of adaption and is well refined to capture the model's signature. Figure 13 shows the number of cells at every adapt cycle, as well as the convergence of the pressure integral along the line sensor, the corrected functional, and an estimate of the remaining error on each mesh. These plots show that the pressure signature is approaching mesh convergence.

USM3D was used to obtain an inviscid solution on a 72 million-cell grid. Figures 14 and 15 show symmetry plane grid colored by pressure coefficient and overlaid constant pressure lines for a USM3D solution of the LBC in free air at M=1.6 and $\alpha = 0.3^{\circ}$. The signature was computed at 1.7 body lengths below model. Experimental data with a USM3D inviscid simulation and CART3D is shown in Fig. 16. There is good agreement with experiment in the forward portion of the pressure signature but poor agreement in the aft region. Similar behavior was reported by other LBC researchers[1-1]. In an attempt to better capture the aft part of the signature and to investigate the effect of viscous modeling on the prediction of the sonic boom signature, USM3D viscous simulations were conducted. A Navier-Stokes near-field grid was generated using VGRID and then a MCAP mesh was attached in a similar fashion as the Euler grids. The original grid had 53 million cells. Figure 17 shows the symmetry plane solution near the configuration. A refined 130 million cell grid was generated and used to adequately model viscous and turbulence effects is shown in Fig. 18. The figure shows the USM3D SST symmetry plane solution near the configuration. The lines of constant pressure are parallel to the shearing angle indicating that the shocks are aligned with the mesh, thus providing confidence in the solution. The viscous solutions with the two different grids are compared with experimental data in Fig. 19. The viscous solution on the 53 million cell grid appears to capture the entire forward signature through the expansion at the y=0 axis. The aft signature does not agree well with the experimental results due to insufficient grid used near the aft region of the model. The finer grid calculates the aft part of the signature substantially better and closer to the WTT data which emphasizes the importance of the grid density in predicting low boom signatures.

A fully turbulent solution and a laminar solution were obtained on the fine grid. The Menter SST model was used to model turbulence. Figure 20 shows comparison of USM3D viscous and inviscid solutions and the UPWT data for the model in free air. The viscous computations accurately captures the entire signature. The rear portion of the signature now agrees well with experiment, whereas the inviscid solution has poor agreement in the aft region. The inviscid pressure signature deviates from the viscous and wind tunnel signatures at X/L=2.65 which corresponds to the region of main compression on the wing. Viscous calculations slightly underestimated the strength of the wing expansion and recovery. The pressure signature obtained using the SST turbulence model provided the best correlation with the UPWT data. Figures 21 and 22 compare experimental off track pressure signatures with USM3D off track viscous signatures. The ability to predict the nose shock as well as shown here is a significant accomplishment because the MCAP computational mesh was constructed to radially align on-track and off-track[10]. The reason that viscous models did not fully capture the wing expansion is unknown and might be attributed to the effects from the wind tunnel flow-field on the model. In the next section an attempt to calculate the LBC in the NASA Langley UPWT will be presented.

B. Empty Tunnel

Empty UPWT simulations were performed with USM3D and AERO. These calculations were conducted to evaluate flow angularity and quality of the flow inside the tunnel. Figure 23 shows a cross sectional view of grid colored by Mach contours inside the UPWT at M=1.6 and Re_L = 3.85x10^6 for a USMD computation. The flow angles, (ϑ_v) and (ϑ_H) measured in the horizontal plane in the center of the test section of the UPWT are shown in Figure 24 for the USM3D code using the SST turbulence model. The flow angle ϑv varies by less than 1° degree in the test section and less than 0.4° in the horizontal plane (z = 0 plane), while ϑ_H varies by less than 0.05°. The range of the computed flow angularities, ϑ_H and ϑv, in the test section are in good agreement with tunnel calibration results[1]. The empty tunnel flow was also computed by AERO and the adapted grid after 13 cycles of adaption had approximately 114 million cells. The initial mesh had 20,857 cells. Cross-section view of the pressure coefficient contours in the UPWT as computed by AERO are shown in Figure 25. A single line sensor placed 10.5 inches from the tunnel wall (1.7 body lengths below the nominal model location) was used as the functional for adaptation within AERO. Note the non-uniform pressure distribution upstream of the test section, i.e. upstream of the line sensor. The color contours are set so that as the flow reaches the test section Mach number of 1.6, the colors transition from red to yellow. This variation in the pressure coffecient along the line sensor is shown in Figure 26 for the final four adaptation levels. The signature is reasonably well converged by the tenth adaptation cycle although some fine-grain features emerge over the next three iterations. Finer triangulation of the tunnel's interior is required to proceed further. In order to obtain the pressure signatures of the model within the tunnel we subtract the tunnel empty signature (adapt 13 in Fig. 26) from the signature obtained when the model is present. Note that all pressures are normalized by the reference pressure (P_r) prior to the subtraction. Lastly, Figure 27 shows the number of cells at every adapt cycle, as well as the convergence of the pressure integral along the line sensor, its adjoint correction, i.e. the value of the pressure integral if the mesh was uniformly refined, and an estimate of the remaining error on each mesh. The plots indicate that the problem is well behaved and approaching mesh convergence.

C. LBC in UPWT

During the WTT, the model was moved forward in 0.125 inch increments while the model pressure signature data were obtained from the reference and survey static pressure probes. Data were acquired in a move/pause mode of operation. For each pressure signature run, the model was moved approximately 24 inches. The CFD analysis was intended to mimic the WTT procedure, thus computations of the model, at four axial locations covering the range of the models positions during the test, were computed and compared to the wind tunnel data. Furthermore, the WTT pressure probes were at a distance of 10.5 inches from the wall and therefore, the line sensors were placed at the same offset from the tunnel wall for the CFD calculations. Figure 28 shows overall view of UPWT with model (enlarged) to show the scales involved in the computation. The tunnel walls are colored by Mach number contours from the AERO calculation.

TetrUSS (USM3D)

USM3D simulations of flow around the LBC in the wind tunnel was a challenging task due to difficulties in generating a suitable computational grid. As discussed in the previous section, preserving shock waves for multiple body lengths without dissipation requires a fine stretched grid that is aligned with the direction of the shock. This helps reduce diffusion of the shock in the computational domain and thus enables the numerical scheme to accurately predict the sonic boom signature away from the body. VGRID and POSTGRID had difficulty producing grids with high stretching ratios inside the wind tunnel because the advancing-front algorithm as implemented is not stable for such stretching. The problem is even more difficult when large volumes are required in order to capture shocks away from the vehicle. Figure 29 shows a cross section view of the grid colored by overpressure coefficient contours for the LBC inside the UPWT at test section Mach number =1.6, H/L = 1.7, and α=0.3° for the USM3D inviscid solution on a 74 million cell grid. The arrow in the figure points to the location of the pressure probe in the tunnel. The grid was deemed too coarse for this sonic boom calculation. Currently, work is being pursued to generate a grid similar in quality to the grid generated by MCAP method. In a parallel effort, the authors are also investigating Chimera overset-grid capability within USM3D as well as hybrid methods to compute flow around the LBC in the tunnel.

AERO

The flow computations from AERO of the LBC in the UPWT were evaluated at four axial locations, at Xnose of -5, 0, 5, and 10 inches, in addition to the empty tunnel run. The line sensor location was 1.7 body lengths below the model. All 4 solutions achieved thirteen levels of adaption and reached over 110 million cells. Figure 30 shows a cut-away view of the test section with one side wall removed and the remaining walls colored by the DP/P along with a flowfield slice through the model. The pressure contours after thirteen adaptation cycles for the model at x = 5 inches solution are shown. The refinement pattern shows a relatively fine mesh extending upstream of the model and line sensor, indicating that this region of the tunnel flow has a relatively large influence on the pressure signal. Figure 31 shows the intial coarse mesh with 20,000 cells in the test section of the tunnel and the final mesh with 130 million cells for AERO results of LBC at location x = 0 in tunnel. The refinement above and in front of model, and below and in front of the sensor higlights the importance of the upstream flow on the pressure signature. Figure 32 shows a comparison between the computed pressure signatures of the LBC in the UPWT at the four axial locations with the WTT data. AERO results captured nose shocks and the salient features of low boom signatures. The boom signature changes with model position due to pressure variation in the tunnel. The signatures agree fairly well in the ambient region of the line sensor. Some differences are observed in the region of the main wing expansion, $1.0 < X/L < 1.5$. These variations in pressure signatures could be a limiting factor for the accuracy of sonic boom wind tunnel test data. An additional refinement level was performed for the X=0.0 case. The final mesh contains approximately 135 million cells and as shown in Fig. 33. The agreement in the aft signature improves, but some disagreement persists with both experimental results at X/L of 2.75. This is a subject of an ongoing investigation**.**

Schlieren Flow Visualization

After completion of the WTT, Schlieren photographs of the model were obtained. During this test, the Schlieren system knife-edge was oriented approximately parallel to the free-stream flow to highlight density gradients in the vertical direction. For this knife-edge orientation, increasing density gradients in the upward direction appear as white areas in the photographs. Figure 34 shows comparison between UPWT Schlieren photograph and computed density gradients for both AERO and USM3D solutions of the LBC in UPWT at a Mach number of 1.6. The vertical black regions in the UPWT Schlieren photograph are the test section window support bars. The USM3D computed density gradients faded out as we moved away from LBC while the AERO system preserved signature features. Although USM3D accurately captured the sonic boom signature in free air, the volume grid for the model in tunnel diffused the sonic boom signature. This shows the importance of creating fine, stretched and shock aligned grid cells to calculate sonic boom signatures. The AERO package automatically provides this quality of cells because it relies on the solution of an adjoint equation and provides error estimates that can be used to both improve the accuracy of the functional and guide a mesh refinement procedure.

V. Conclusion

A wind tunnel test was conducted by Gulfstream Aerospace Corporation to measure the sonic boom signature of a low boom configuration in the Langley Unitary Plan Wind Tunnel at Mach numbers of 1.60 and 1.80. Two widely used NASA codes, TetrUSS and AERO were used to compute the sonic boom signature of the low boom configuration in free air as well as in the wind tunnel at a free-stream Mach number of 1.6, an angle of attack of 0.3°, and a Reynolds number of 3.85×10^6 based on the model reference length of 13.2 inches. Inviscid, laminar and turbulent solutions were computed with USM3D. Menter SST model was used to model turbelnce. The effects of viscous and turbulence modeling along with the presence of the wind tunnel walls on the computed sonic boom signature were presented. On- and off-track sonic boom signatures were computed and compared to wind-tunnel test data. The correlation with wind-tunnel data showed that sonic boom signature captured by the SST model was the closest to the WTT data. Mach-cone aligned prism cells provided accurate on-track and off-track pressure signatures. Fine, stretched, and shock aligned grids are key parameters in capturing low boom signatures.

The AERO package successfully computed low-boom signatures of the LBC in free air and at four axial locations in the tunnel. This work proved the ability of the adjoint-based mesh adaptation method to guide refinement and control discretization errors in inviscid simulations in the tunnel. The authors are currently involved in generating a complete data set of a sonic boom wind tunnel test that was conducted in the NASA Ames 9- by 7-Foot Supersonic Wind Tunnel. Future work to incorporate the Mach cone aligned prism cells program into a grid generation tool suite developed at NASA Langley Research Center, to generate viscous near body grids with cylindrical boundaries is being planned. The use of USM3D Chimera overset-grid capability to overcome difficulties of generating fine-stretched grids inside the tunnel, is also being considered.

Acknowledgments

The authors would like to thank Donald A. Durston and Scott D. Thomas of NASA Ames Research Center for their valuable comments and long hours of discussion through out the course of this work. Authors thank Norma Farr and Michael Wiese of the Geometry Laboratory at NASA Langley Research Center for developing surface and volume grids.

References

[1] Wilcox, F. J.; and Elmiligui, A. A.: "Experimental Sonic Boom Measurements on a Mach 1.6 Cruise Low-Boom Configuration," NASA TM to be published.

[2] Wayman, T., Howe, D., Waithe, K., Bangert, L., and Wilcox, F.: "Near Field Acoustic Test on a Low Boom Configuration in Langley's 4 x 4 Wind Tunnel," 29th AIAA Applied Aerodynamics Conference, Honolulu, HI, June 2011.

[3] Durston, D. A., Cliff, S. E., Wayman, T., Merret J., Elmiligui, A., and Bangert, L.: "Near-Field Sonic Boom Test on Two Low-Boom Configurations Using Multiple Measurement Techniques at NASA Ames," 29th AIAA Applied Aerodynamics Conference, Honolulu, HI, June 2011.

[4] Carter, M. B., Campbell, R., and Nayani, S.: "USM3D Analysis of a Low Boom Configuration," 29th AIAA Applied Aerodynamics Conference, Honolulu, HI, June 2011.

[5] Howe, D.: "Hybrid CART3D/OVERFLOW Near-Field Analysis of a Low Boom Configuration with Wind Tunnel Comparisons," 29th AIAA Applied Aerodynamics Conference, Honolulu, HI, June 2011.

[6] Park, M.: "Low Boom Configuration Analysis with FUN3D Adjoint Simulation Framework," 29th AIAA Applied Aerodynamics Conference, Honolulu, HI, June 2011.

[7] Cliff, S., Elmiligui, A., Campbell, R., and Thomas, S.: "Evaluation of Refined Tetrahedral Meshes with Projected, Stretched, and Sheared Prism Layers for Sonic Boom Analysis," 29th AIAA Applied Aerodynamics Conference, Honolulu, HI, June 2011.

[8] Carter, M. B., and Deere, K. A.: "Grid Sourcing and Adaptation Study Using Unstructured Grids for Supersonic Boom Prediction," AIAA Paper 2008-6595, 2008.

[9] Cliff, S., Thomas, S., McMullen, M., Melton, J., and Durston, D.: "Assessment of Unstructured Euler Methods for Sonic Boom Pressure Signatures Using Grid Refinement and Domain Rotation," NASA/TM-2008-214568, September 2008.

[10] Campbell, R. L., Carter, M. B., Deere, K. A. and Waithe, K. A.: "Efficient Unstructured Grid Adaptation Methods for Sonic Boom Prediction," AIAA Paper-7327, Honolulu HI, August 2008.

[11] Frink, N. T., Pirzadeh, S. Z., Parikh, P. C., Pandya, M. J., and Bhat, M. K.: "The NASA Tetrahedral Unstructured Software System," The Aeronautical Journal, Vol. 104, No. 1040, October 2000, pp. 491-499.

[12] Frink, N. T.: "Assessment of an Unstructured-Grid Method for Predicting 3-D Turbulent Viscous Flows," AIAA Paper-96-0292, January 1996.

[13] Nemec, M., Aftosmis, M. J., Murman, S. M., and Pulliam, T. H.: "Adjoint Formulation for an Embedded-Boundary Cartesian Method," AIAA Paper 2005–0877, Reno, NV, January 2005.

[14] Nemec, M., and Aftosmis, M.: "Adjoint Error-Estimation and Adaptive Refinement for Embedded-Boundary Cartesian Meshes," AIAA Paper 2007-4187, 18th AIAA CFD Conference, Miami FL, June 2007.

[15] Nemec, M., Aftosmis, M., and Wintzer, M.: "Adjoint-based Adaptive Mesh Refinement for Complex Geometries," AIAA Paper 2008-0725, January 2008.

[16] Aftosmis, M. J., and Berger, M. J.: "Multilevel Error Estimation and Adaptive H-Refinement for Cartesian Meshes with Embedded Boundaries," AIAA Paper 2002-0863, 40th AIAA Aerospace Sciences Meeting and Exhibit, Reno NV, January 2002.

[17] Jackson, C. M., Jr., Corlett, W. A., and Monta, W. J.: Description and Calibration of the Langley Unitary Plan Wind Tunnel. NASA TP-1905, 1981.

[18] Waithe, K. A.: "Design of a Wind Tunnel Mount for a Low Boom Test" 29th AIAA Applied Aerodynamics Conference, Honolulu, HI, June 2011.

[19] TetrUSS Web page: http://tetruss.larc.nasa.gov/usm3d/index.html, May 2011.

[20] CART3D Web page: http://people.nas.nasa.gov/~aftosmis/cart3d, May 2011.

[21] Pao, S. P.: "USMC6-TetrUSS Grid and Solution Cutter: A Brief Users' Guide," Version 4, NASA LaRC, September 2010.

[22] Samareh, J.: "GridTool, A Surface Modeling and Grid Generation Tool," Proceedings of the Workshop on Surface Modeling, Grid Generation, and Related Issues in CFD Solutions, NASA CP–3291, May 9–11, 1995.

[23] Pirzadeh, S.: "Unstructured Viscous Grid Generation by Advancing-Layers Method," AIAA Journal, Vol. 32, No. 8, pp. 1735–1737, August 1994.

[24] Pirzadeh, S.: "Structured Background Grids for Generation of Unstructured Grids by Advancing Front Method," AIAA Journal, Vol. 31, No. 2, pp. 257–265, February 1993.

[25] Aftosmis, M. J., Berger, M. J., and Melton, J. E.: "Robust and Efficient Cartesian Mesh Generation for Component-Based Geometry," AIAA Paper 97-196.

[26] Pandya, M. J., Abdol-Hamid, K. S., and Frink, N. T.: "Enhancement of USM3D Unstructured Flow Solver for High-Speed High-Temperature Shear Flows," AIAA 2009-1329, January 2009.
[27] Abdol-Hamid, K. S., Frink, N. T., Deere, K. A., and Pandya, M. J.: "Propulsion Simulations Using Advanced Turbulence Models with the Unstructured-Grid CFD Tool, TetrUSS," AIAA 2004-0714, January 2004.
[28] Deere, K. A., Elmiligui, A. A, Abdol-Hamid, K.S.: "USM3D Simulations of Saturn V Plume Induced Flow Separation," AIAA-2011-1055.

Figure 1. LBC mounted in NASA Langley UPWT.

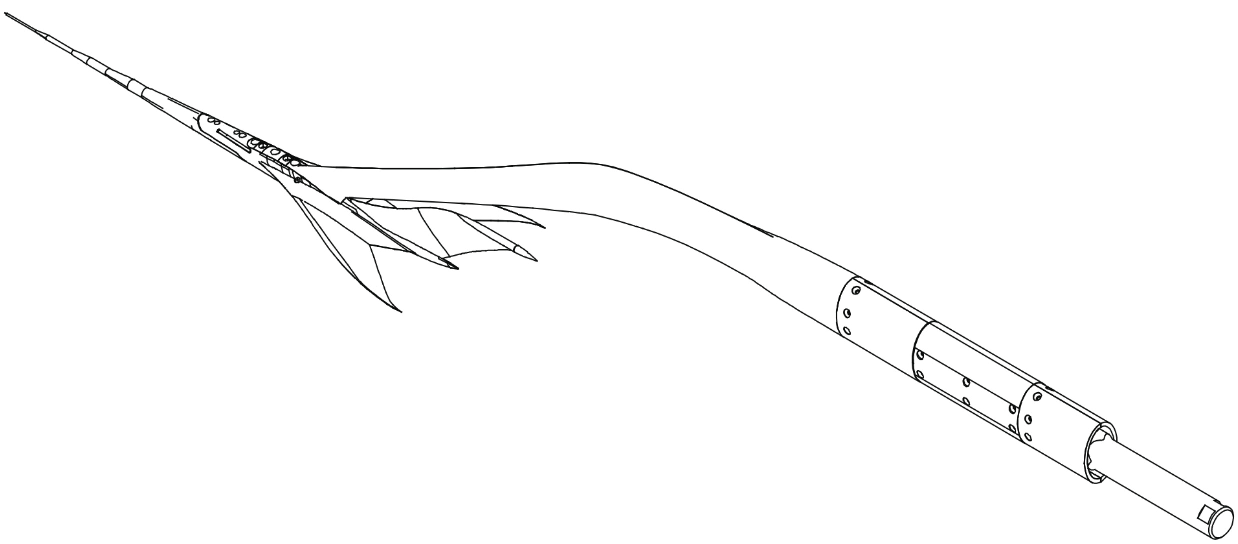

Figure 2. Isometric of LBC and blade sting.

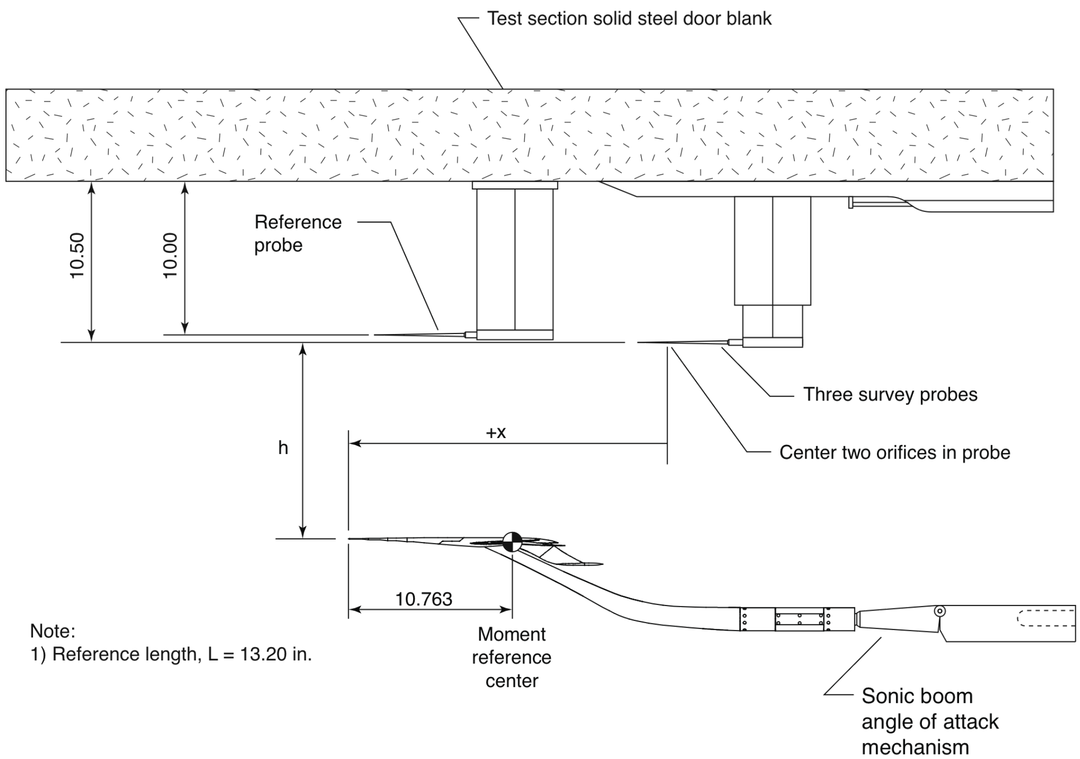

(a) Top View.

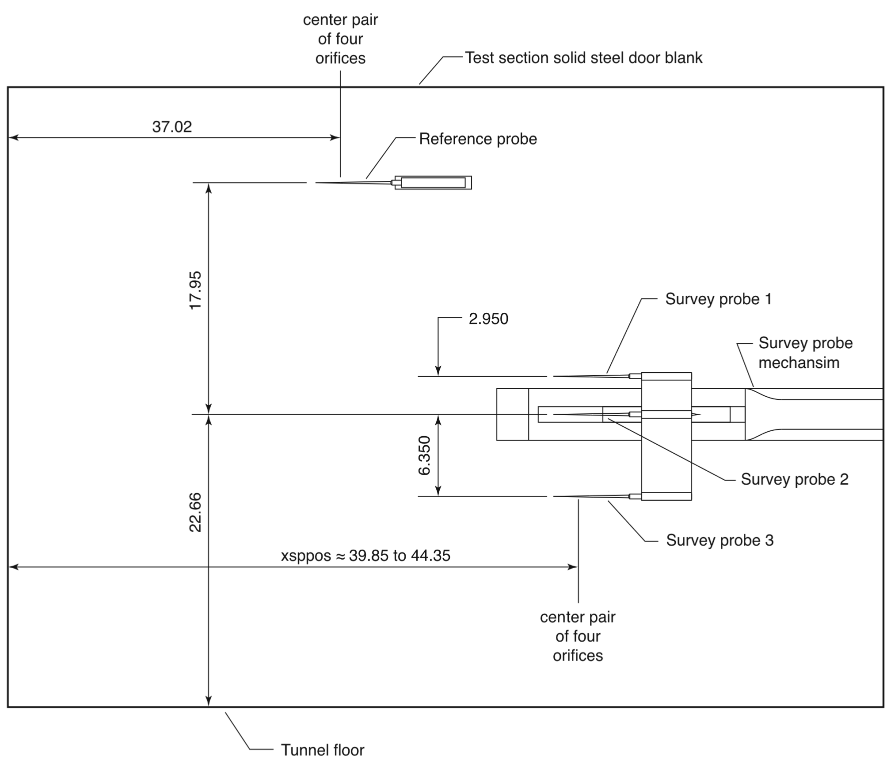

(b) Side View.

Figure 3. Location of reference and survey pressure probes in the UPWT. (All dimensions in inches)

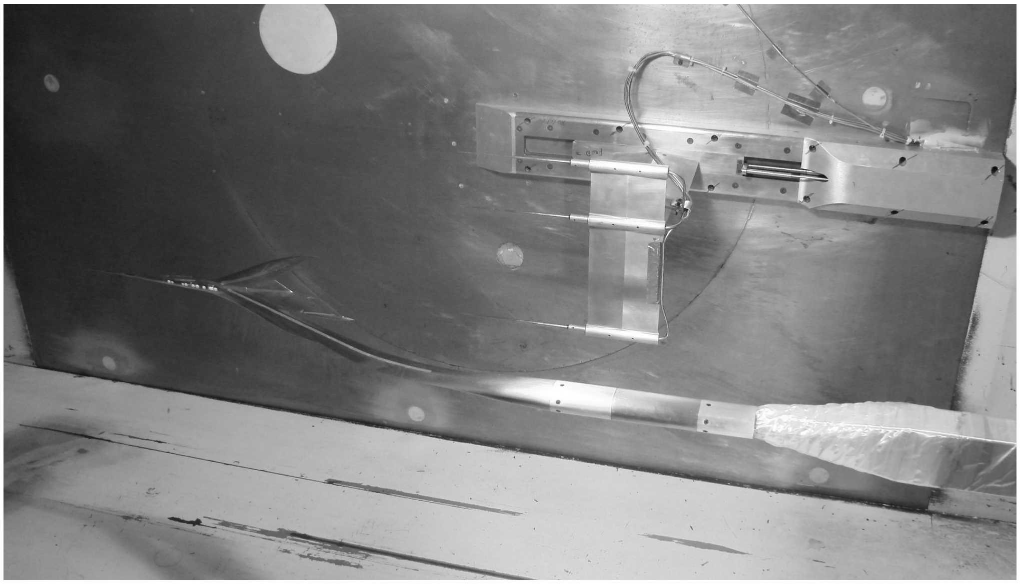

Figure 4. Photograph of the LBC, traverse mechanism, and survey probes mounted in the UPWT.

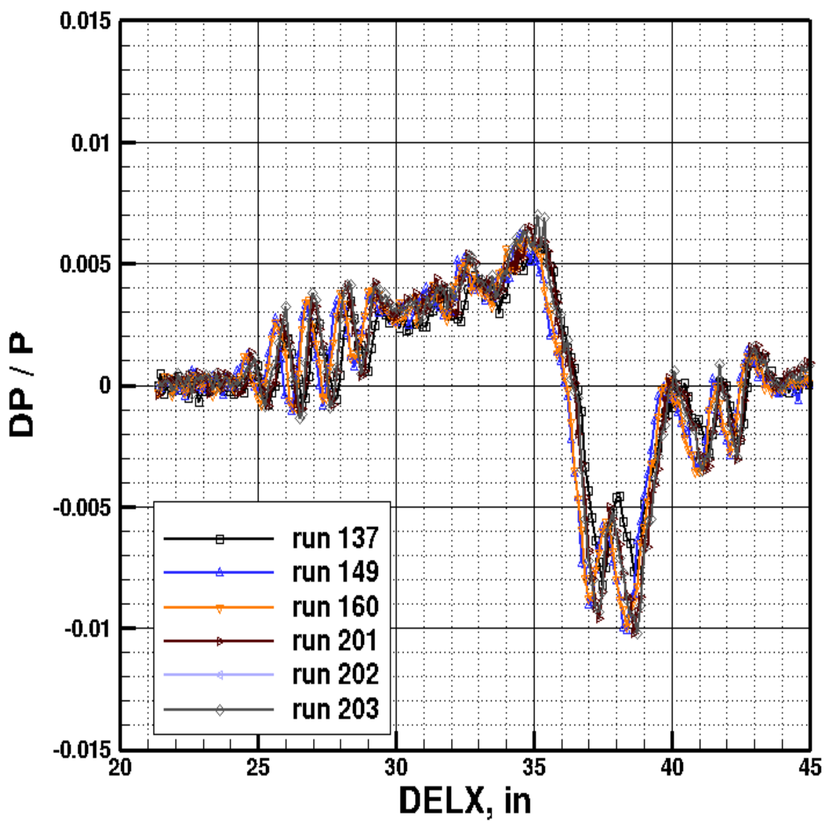

Figure 5. Wind tunnel data repeatability at M=1.6, α =0.25°, H/L=1.7, Xnose = 42.35 inches, Re_L = 3.85x10^6.

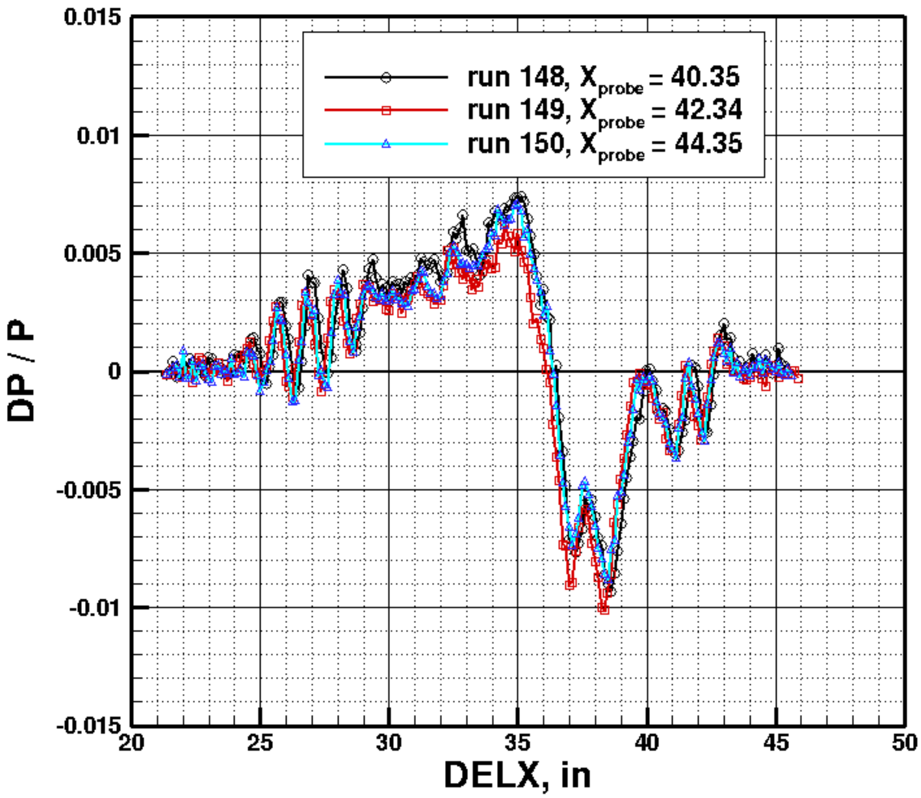

Figure 6. Effect of survey probe position on sonic boom signature at M=1.6, α=0.25°, H/L=1.7, $Re_L = 3.85x10^6$.

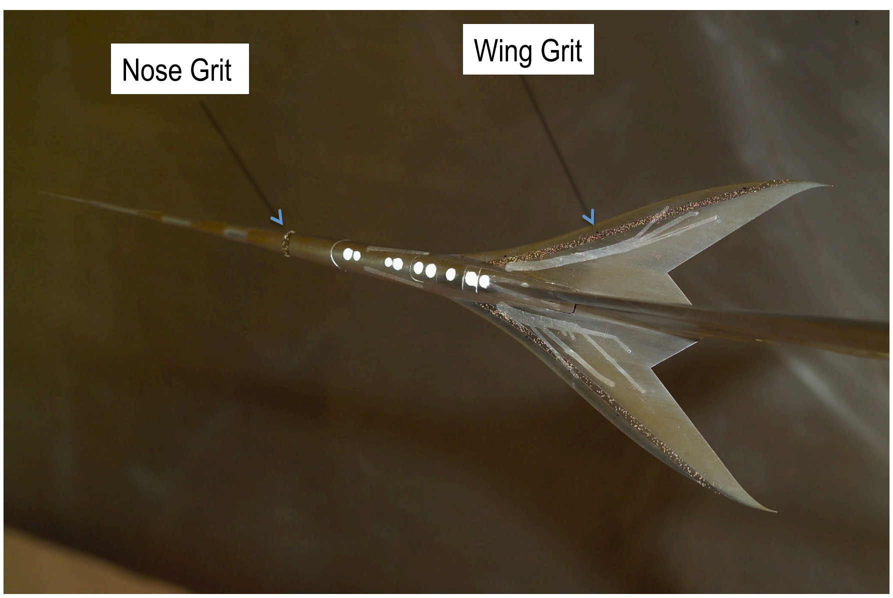

Figure 7. Photograph showing grit location on LBC.

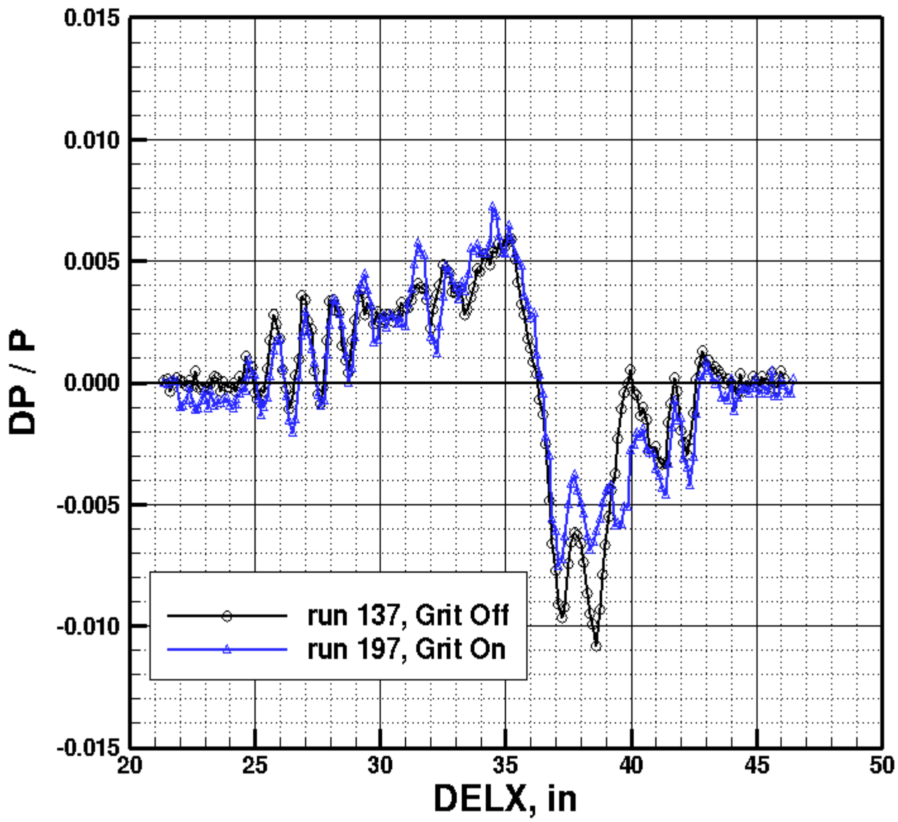

Figure 8. Effect of boundary layer transition grit.

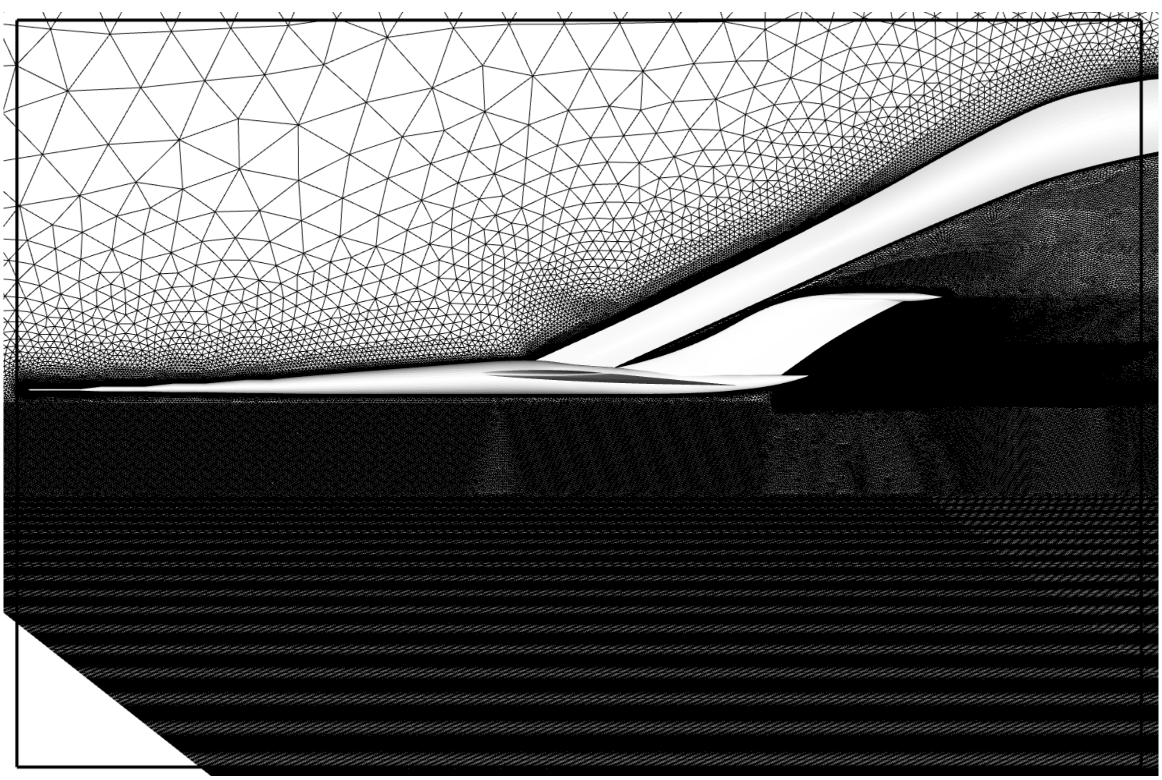

Figure 9. Symmetry plane of the 130 million-cell grid of LBC in free air.

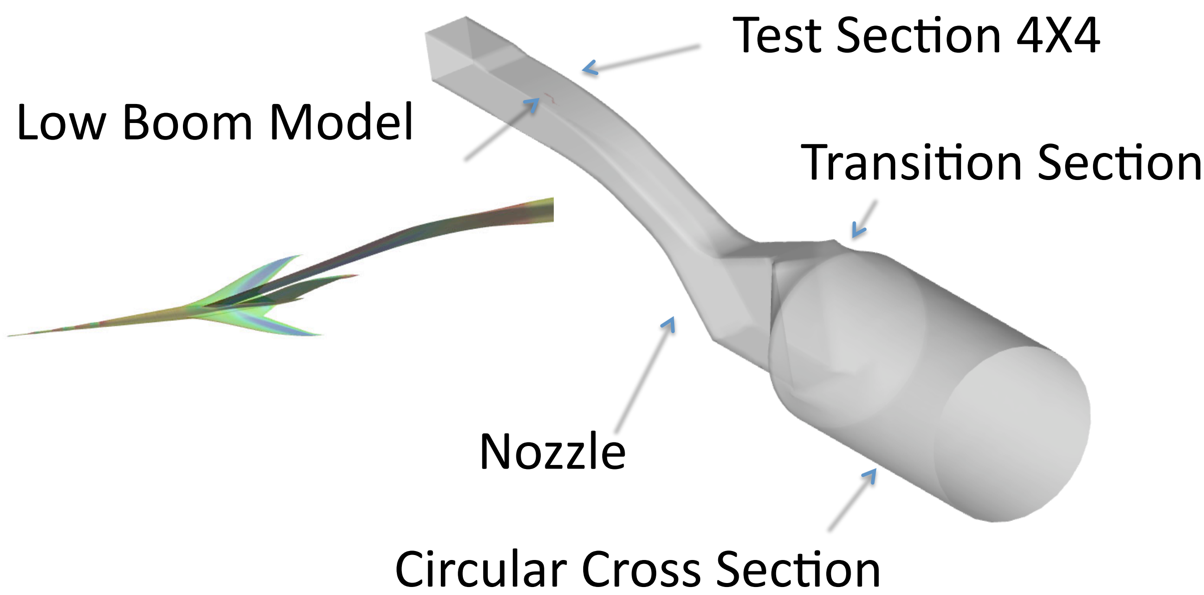

Figure 10. Schematic view of LBC in UPWT.

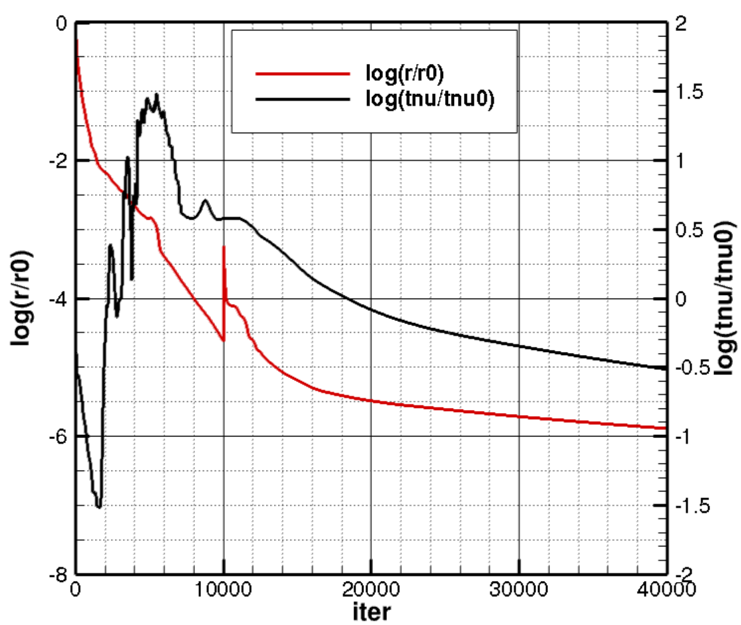

Figure 11. USM3D convergence history.

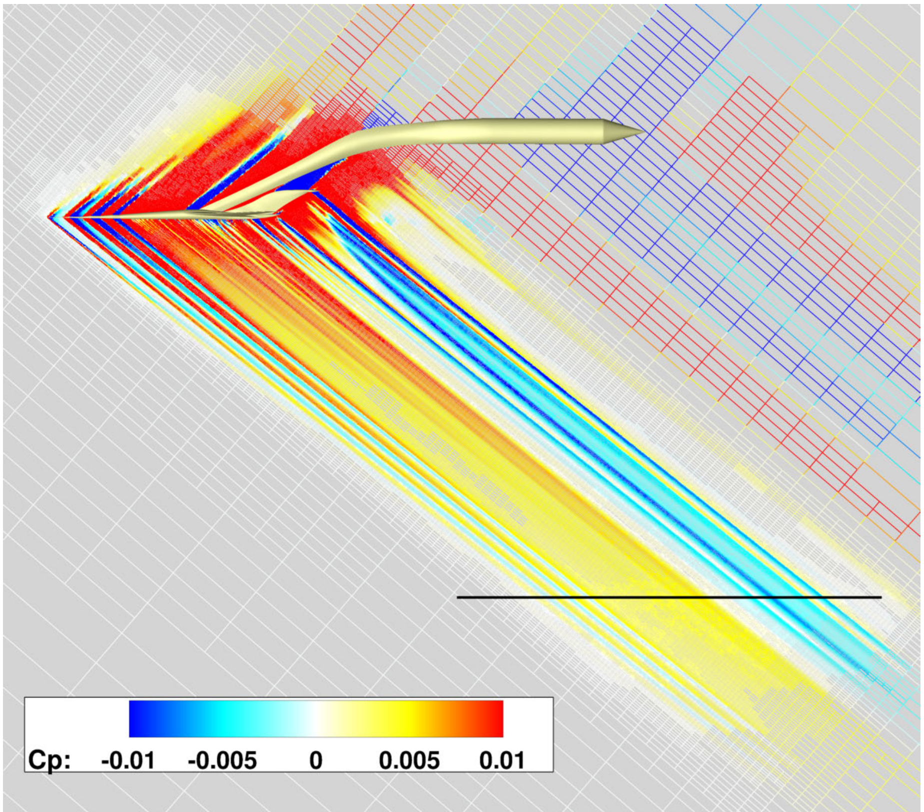

Figure 12. LBC symmetry plane grid colored with Cp.
AERO calculation of the LBC in free air at M=1.6 and α = 0.3º.

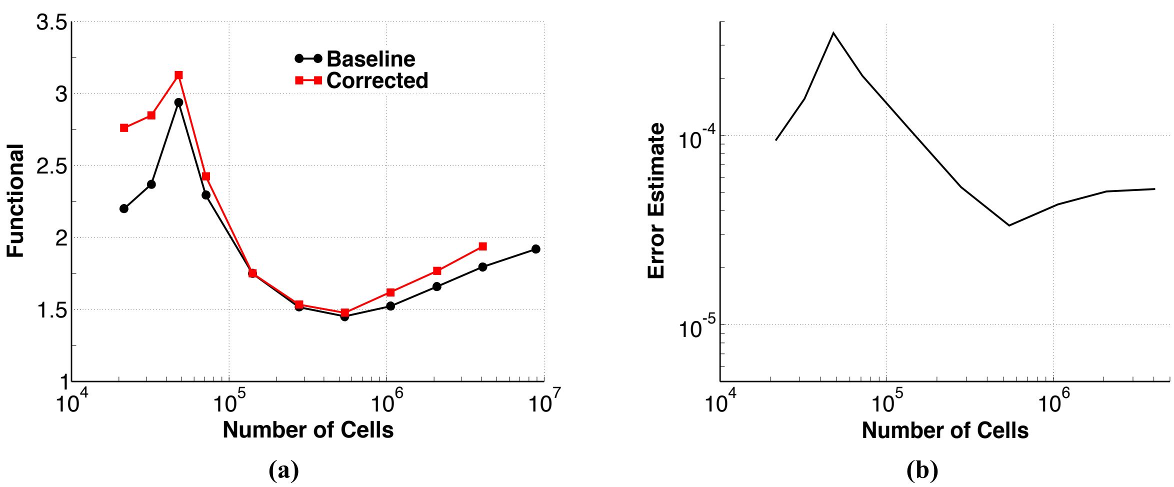

(a) **(b)**

Figure 13 Convergence of functional and remaining error estimate for AERO calculations

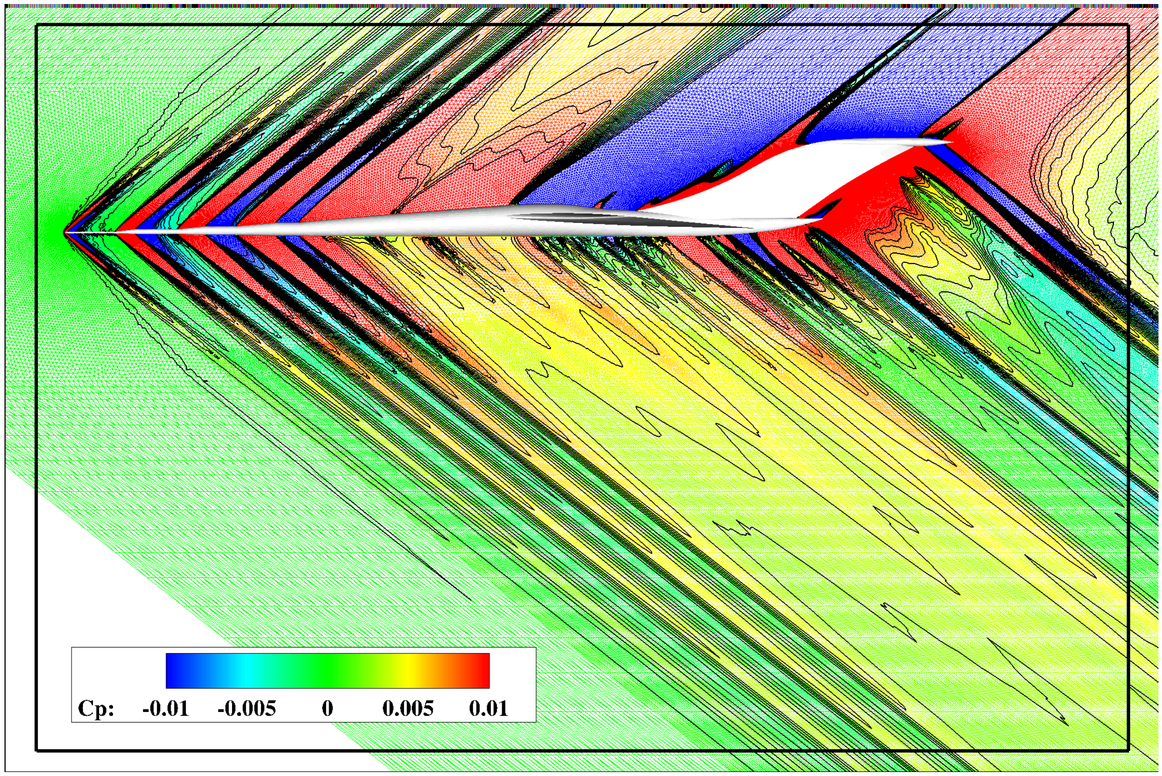

Figure 14. Symmetry plane grid colored by Cp and overlaid with constant pressure lines. USM3D solution of the LBC in free air at M=1.6 and α = 0.3º.

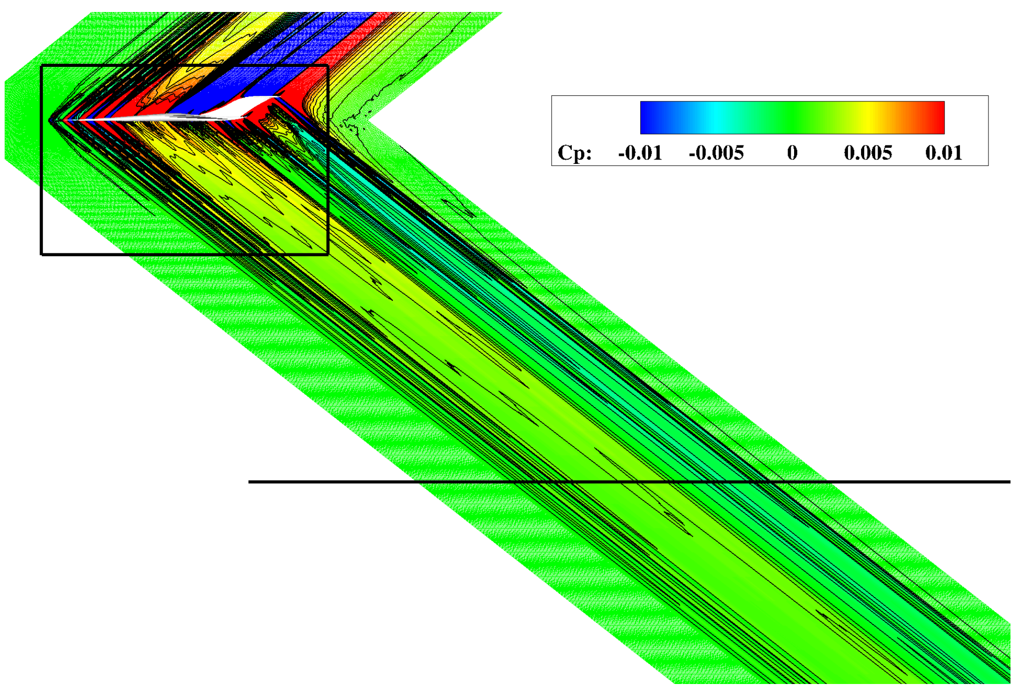

Figure 15. Symmetry plane grid colored by Cp and overlaid with constant pressure lines. USM3D solution of the LBC in free air at M=1.6 and α = 0.3°. Signature sampled at 1.7 body lengths below model.

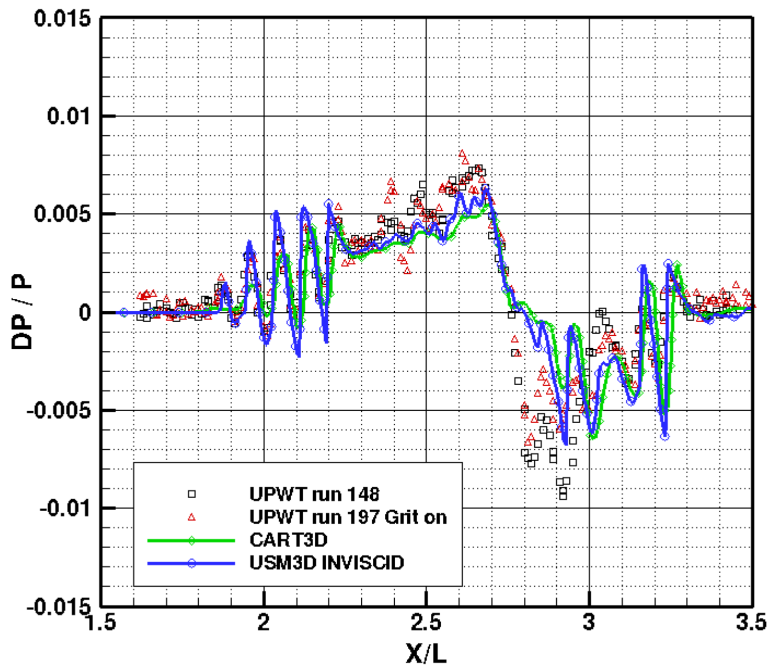

Figure 16. Comparison of inviscid USM3D and AERO data with LARC UPWT data for LBC at M=1.6, α = 0.3°, H/L=1.7, ϕ=0°.

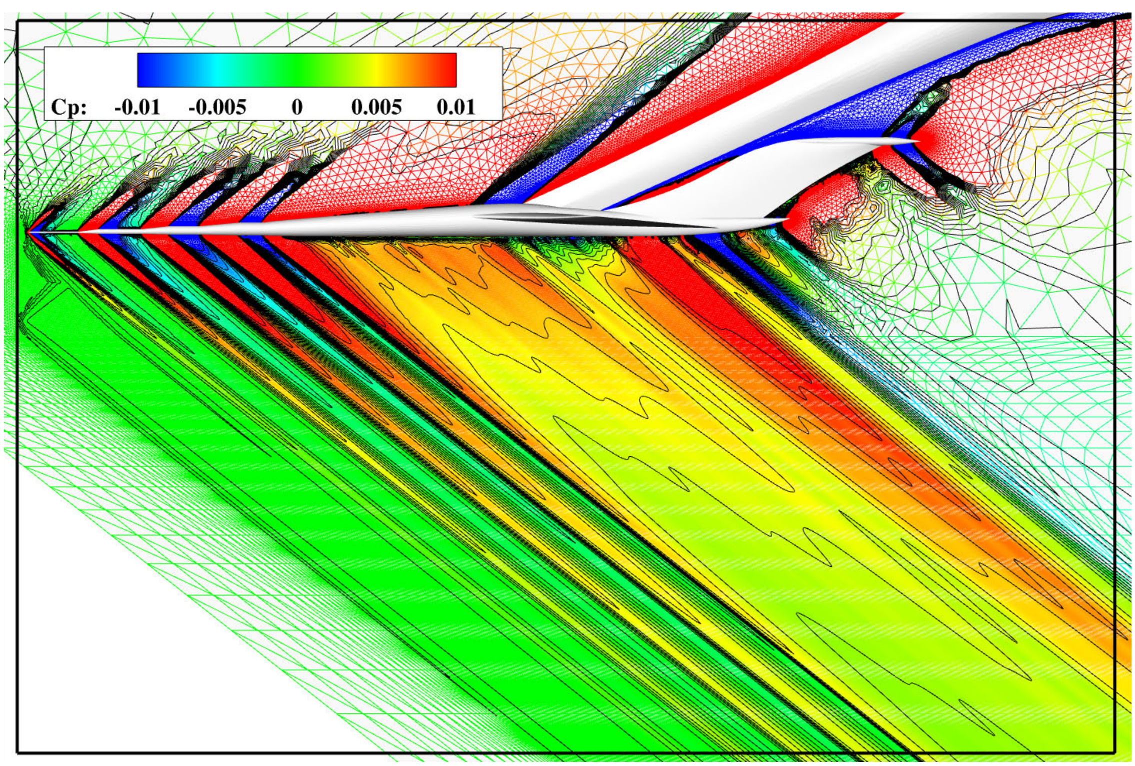

Figure 17. Symmetry plane grid colored by Cp and overlaid with constant pressure lines. USM3D viscous solution of the LBC at M=1.6, α = 0.3°, Re_L = 3.85x10^6. Grid = 53 million cells.

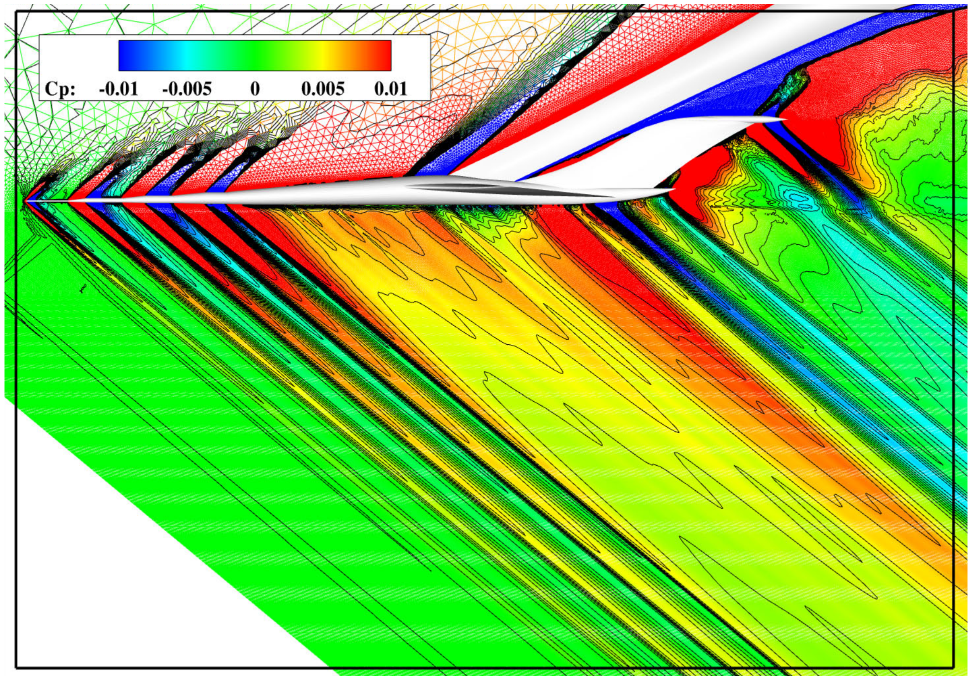

Figure 18. Symmetry plane grid colored by Cp and overlaid with constant pressure lines. USM3D SST solution of the LBC at M=1.6, a = 0.3°, Re_L = 3.85x10^6. Grid = 130 million cells.

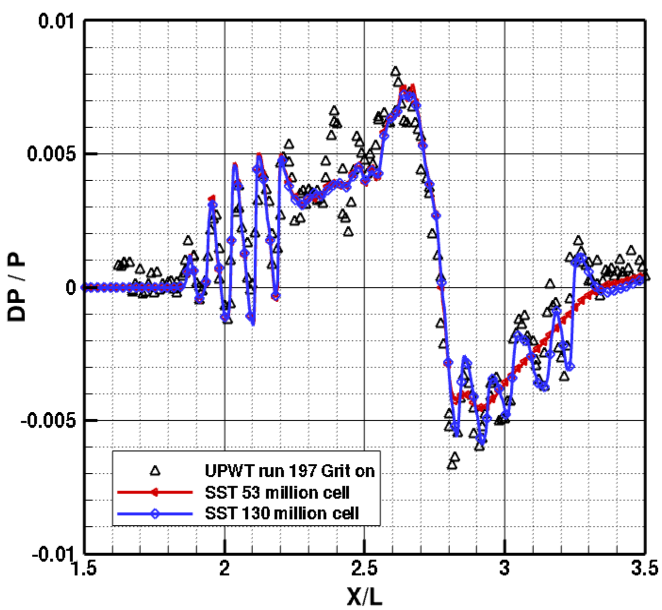

Figure 19. USM3D viscous solution compared with LARC UPWT data at M=1.6, α =0.3°, H/L=1.7, Re_L = 3.85x10^6, ϕ=0°.

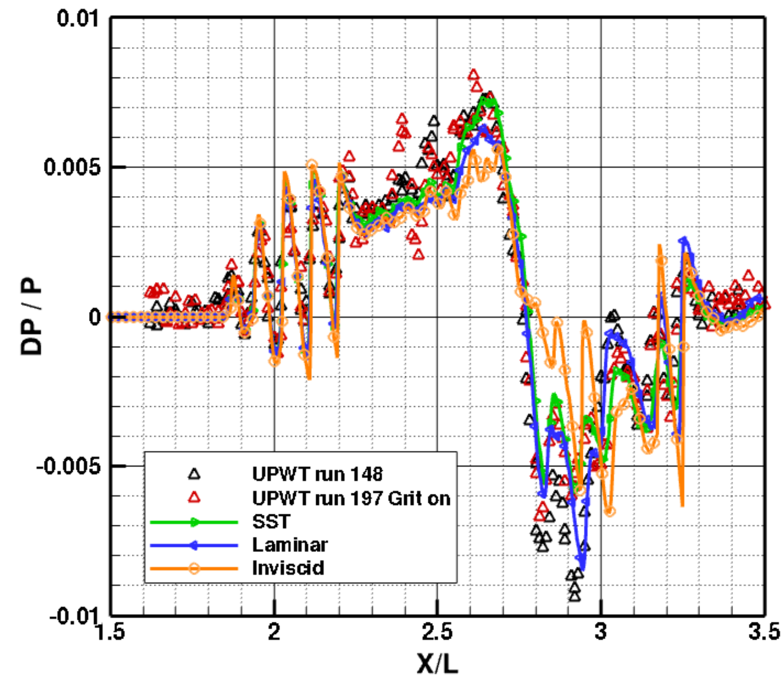

Figure 20. Comparison of USM3D viscous and inviscid simulations with LARC UPWT data at M=1.6, α=0.3°, H/L=1.7, ReL = 3.85x106, φ = 0º. Grid = 130 million cells.

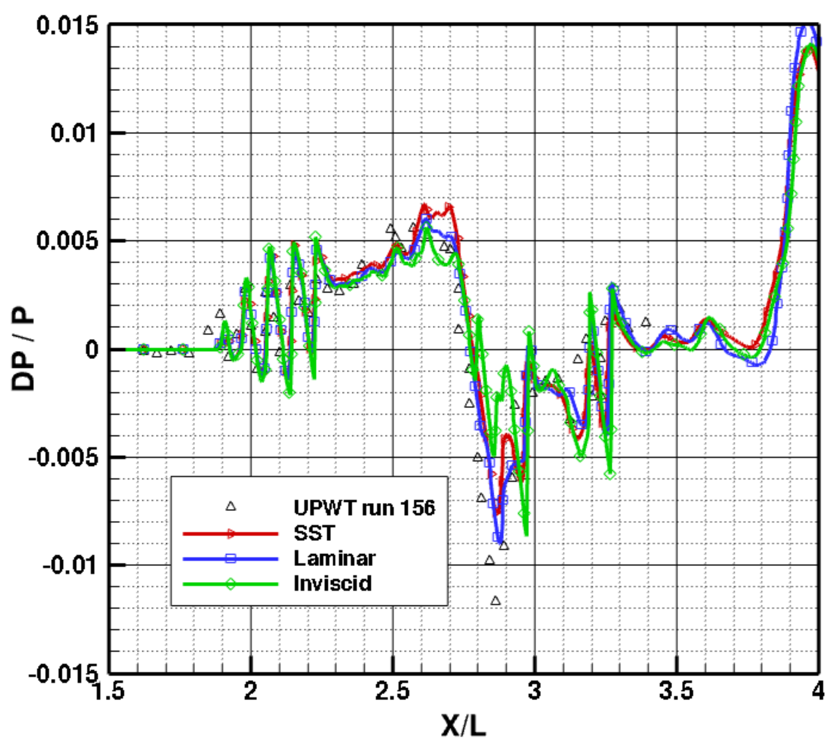

Figure 21. Comparison of USM3D viscous and inviscid simulations with LARC UPWT data at M=1.6, α=0.3°, H/L=1.7, Re_L = 3.85x10^6, ϕ=25.5°.

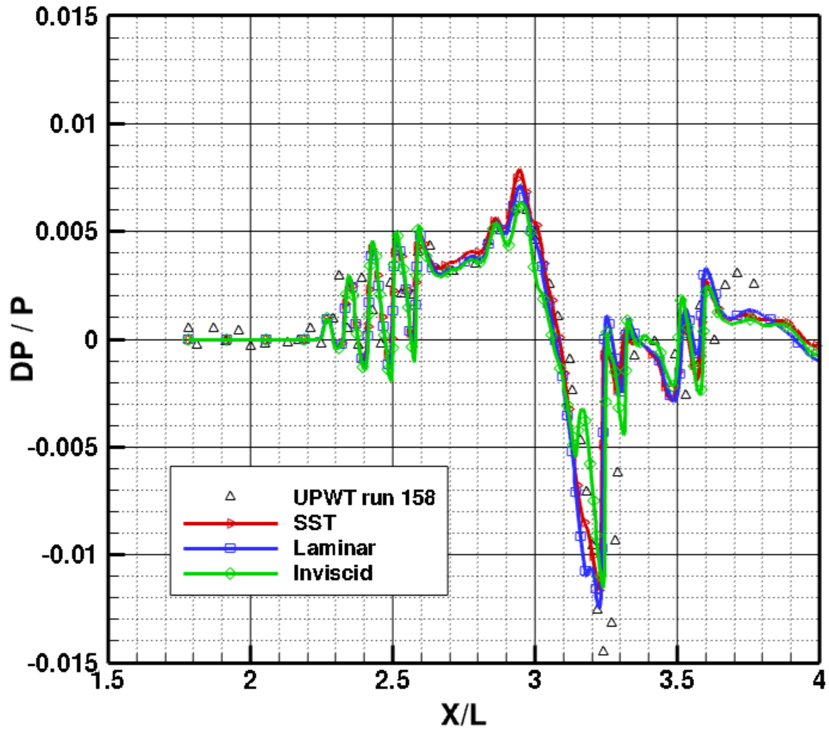

Figure 22. Comparison of USM3D viscous and inviscid simulations with LARC UPWT data at M=1.6, α=0.3°, H/L=1.7, Re_L = 3.85x10^6, ϕ=53.4°.

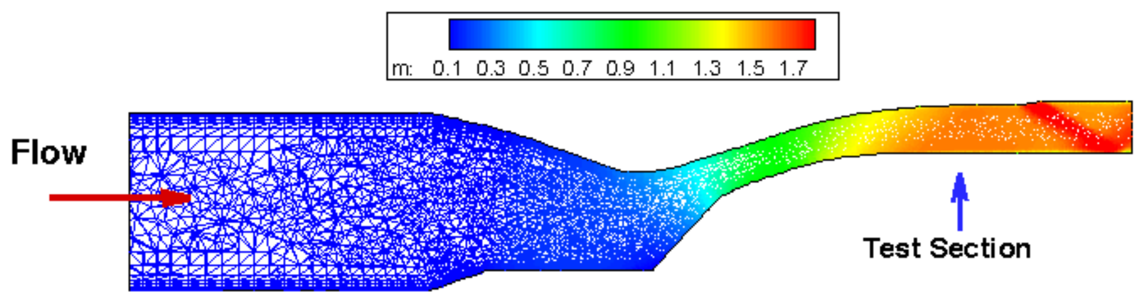

Figure 23. Cross section view of grid colored by Mach contours inside UPWT at M=1.6 and Re_L = 3.85x10^6.

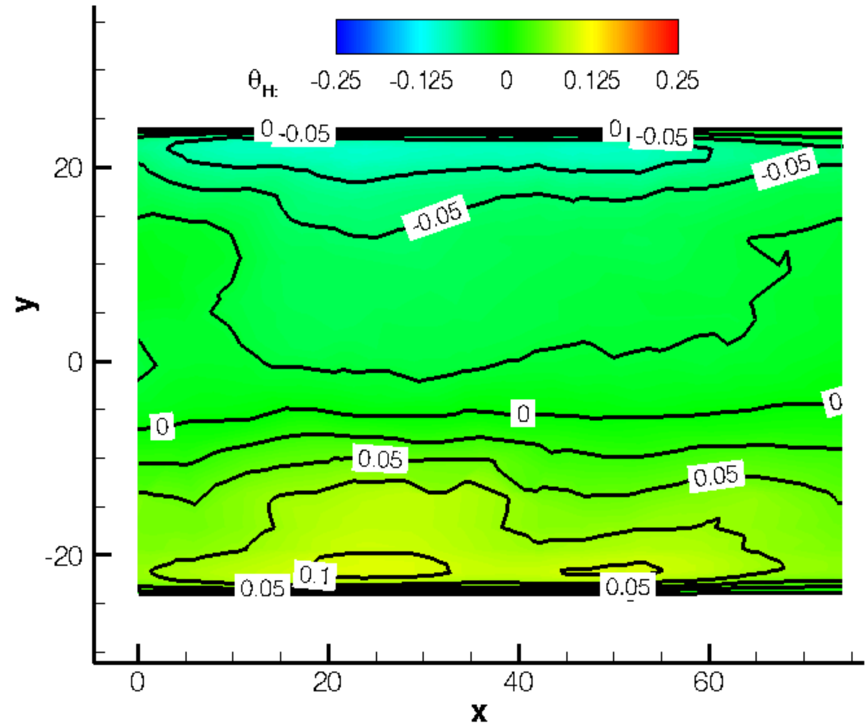

(a) θ_H

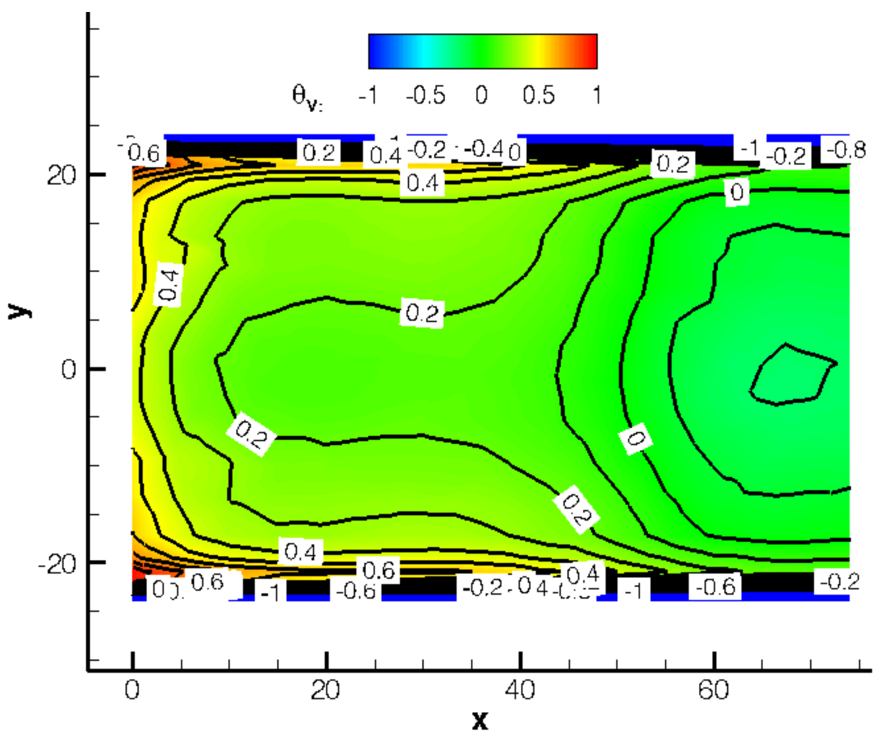

(b) θ_V

Figure 24. Flow angles in the UPWT as computed by USM3D at M=1.6 and Re_L = 3.85x10^6 along the Z = 0 plane.

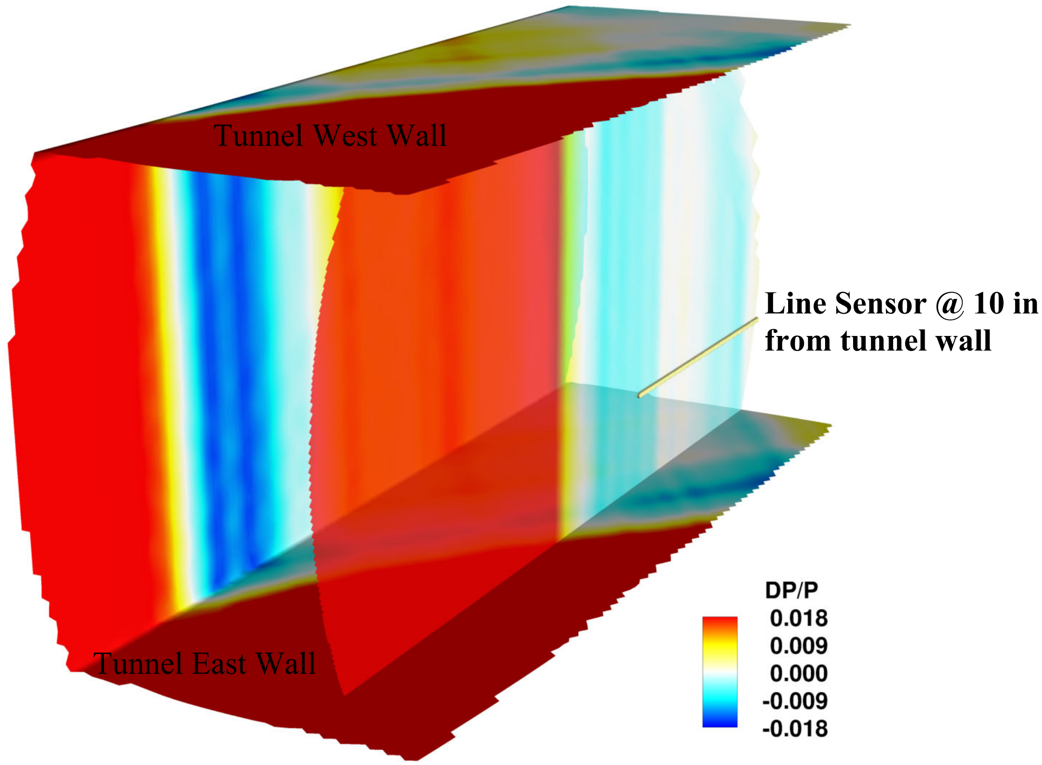

Figure 25. Cross sectional view of pressure coefficient contours in the UPWT as computed by AERO at M=1.6.

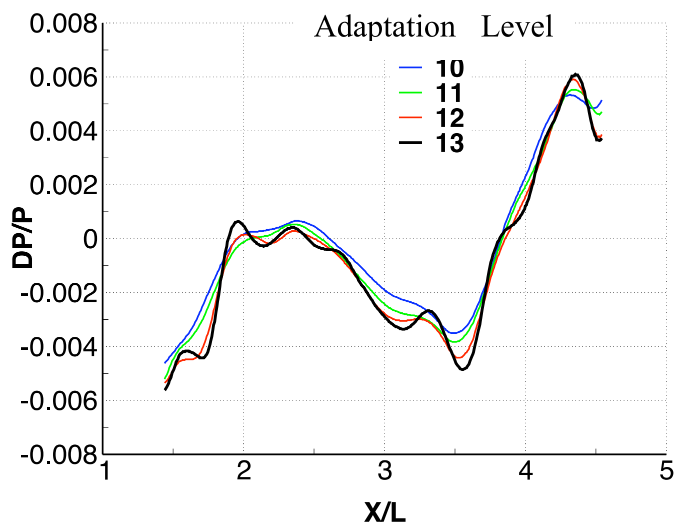

Figure 26. Variation in overpressure coefficient along line sensor for UPWT as computed by AERO at M=1.6.

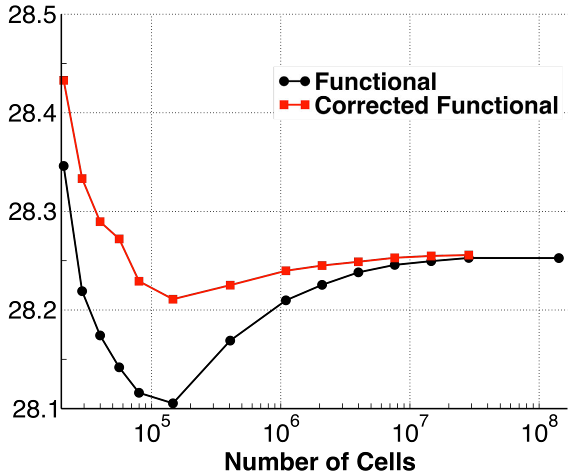

(a)

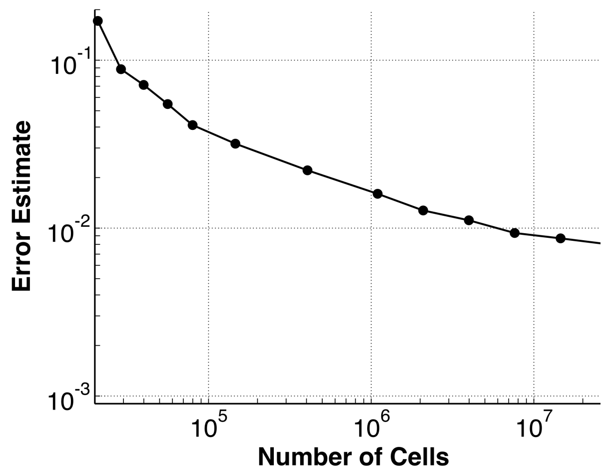

(b)

Figure 27. Convergence of functional and remaining error estimate for UPWT as computed by AERO at M=1.6.

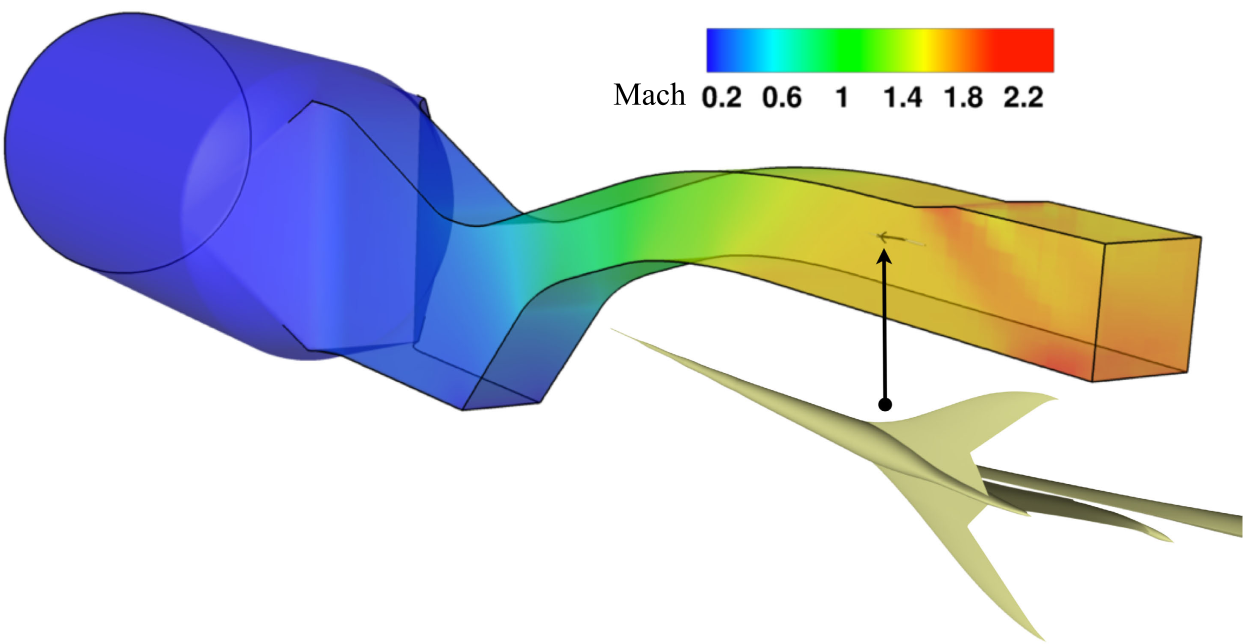

Figure 28. Overall view of UPWT with model (enlarged) to show the scales involved in the computation. AERO solution for the flow in UPWT, tunnel colored by Mach number contours.

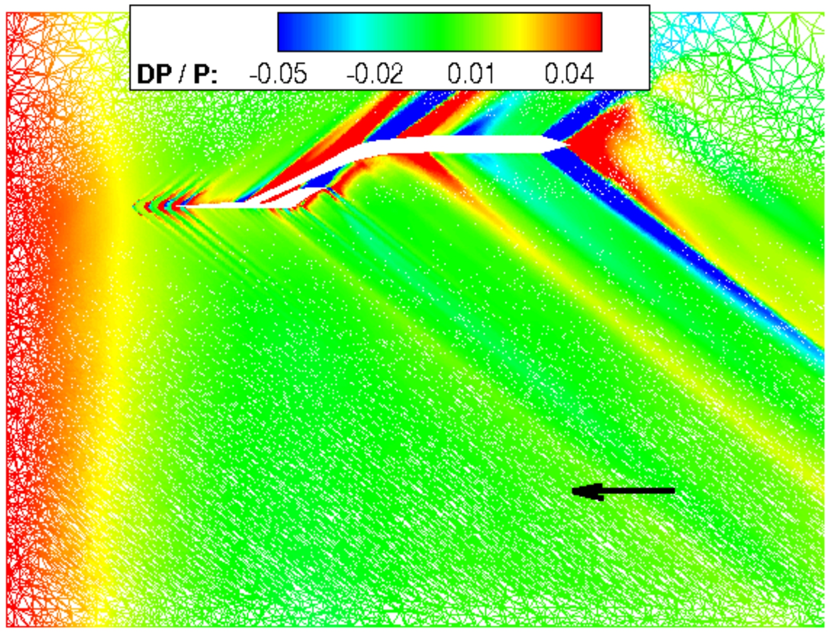

Figure 29. Cross section view of grid colored by overpressure coeficient for LBC inside UPWT at M=1.6, ∝=0.3° and Re_L = 3.85x10^6. USM3D inviscid solution on a 74 million cell grid. Arrow points to the location of survey pressure probe.

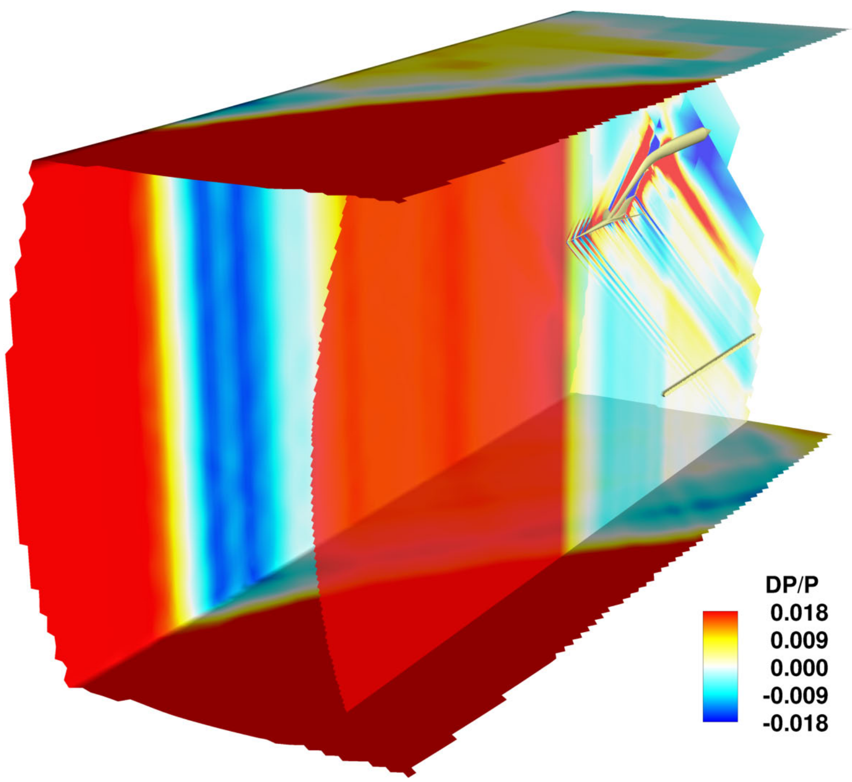

Figure 30. AERO pressure contours of the LBC inside UPWT at M=1.6, ∝=0.3°, H/L=1.7, X_{nose} = 5. inches.

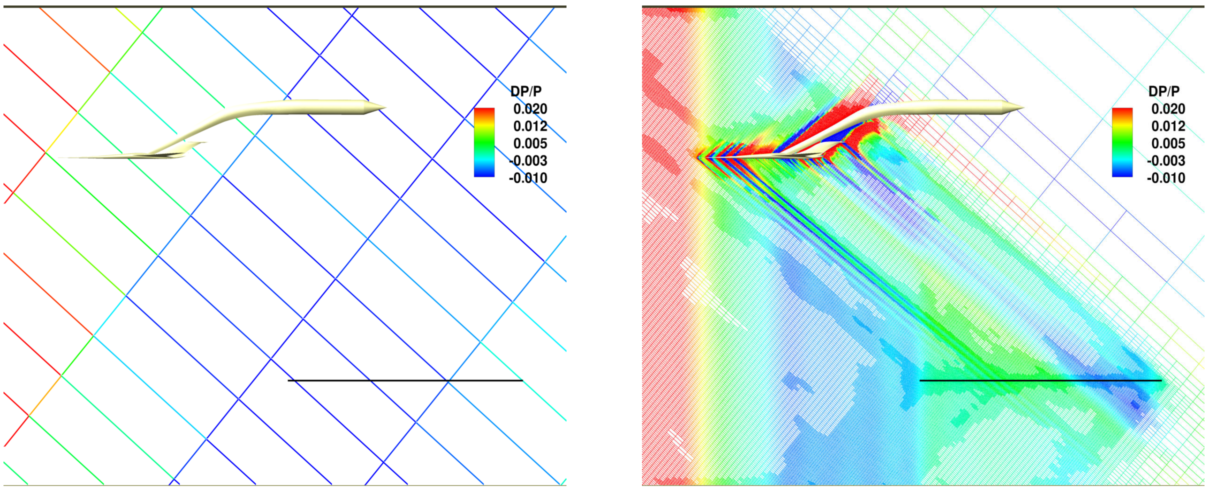

(a) Intial mesh 20,000 cell (b) Final Mesh 130 million cell

Figure 31. AERO intial and final mesh colored by pressure coefficient for the LBC in UPWT at M = 1.6.

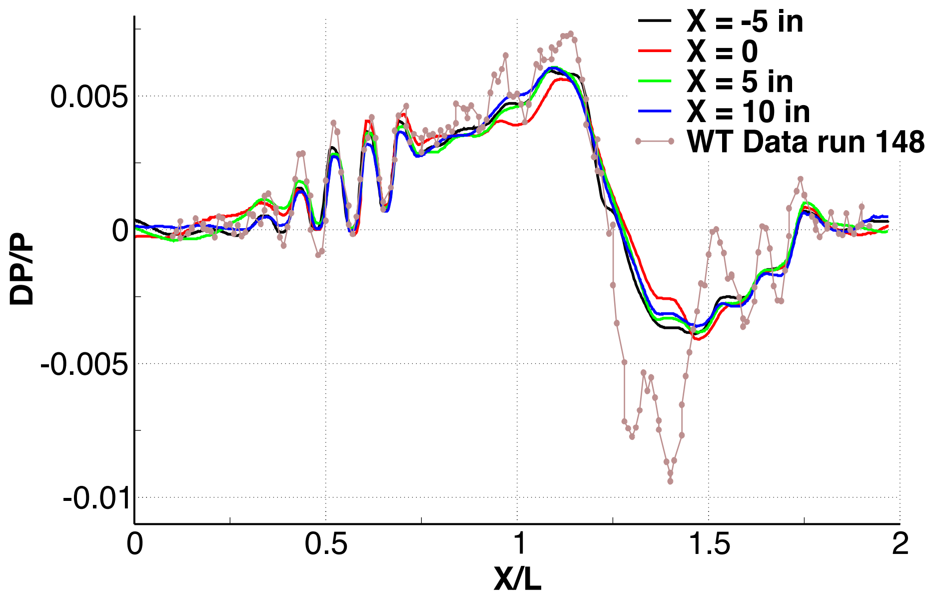

Figure 32. Comparison between AERO computed boom signatures for LBC inside UPWT M=1.6, ∝=0.3°, H/L=1.7.

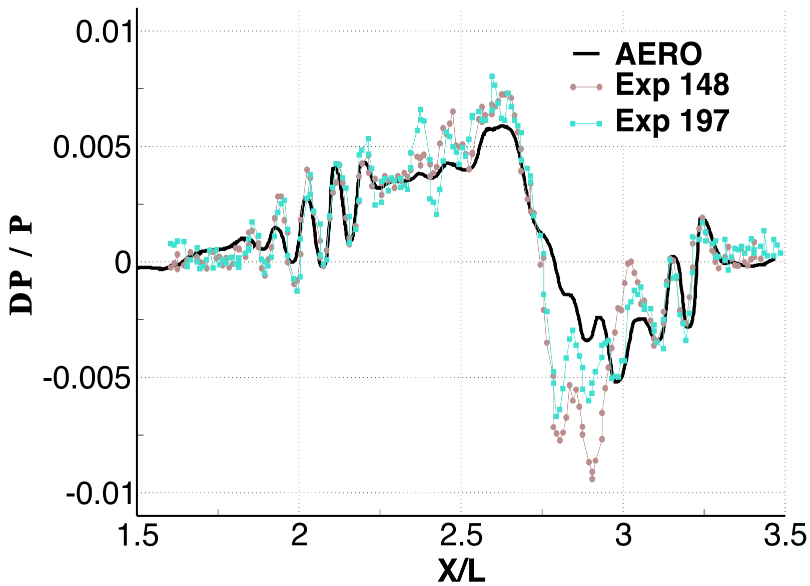

Figure 33. Comparison between AERO computed boom signature at X_{nose} = 0 and WT data for LBC inside UPWT M=1.6, ∝=0.3°, H/L=1.7.

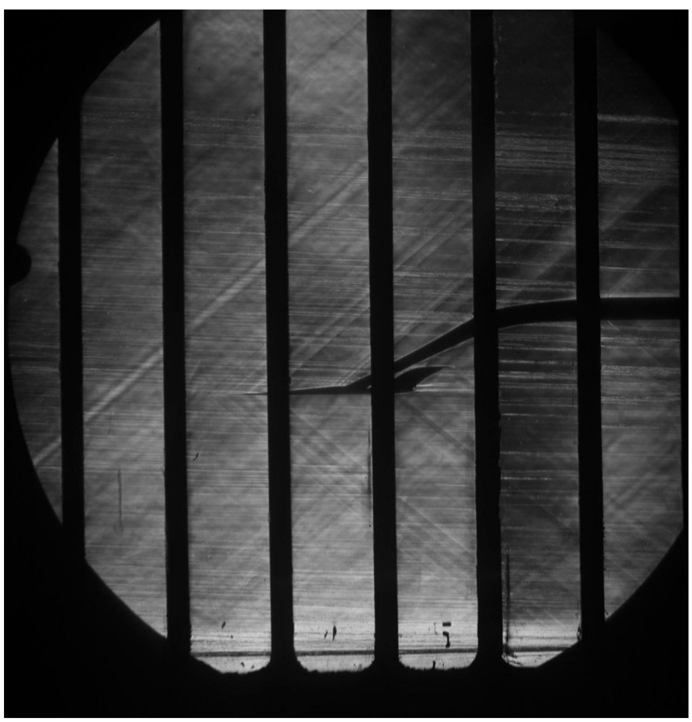

(a) **Wind Tunnel Schlieren Images.**

Figure 34. Comparison of wind tunnel Schlieren images for the LBC inside UPWT and computed density gradients at M = 1.6.

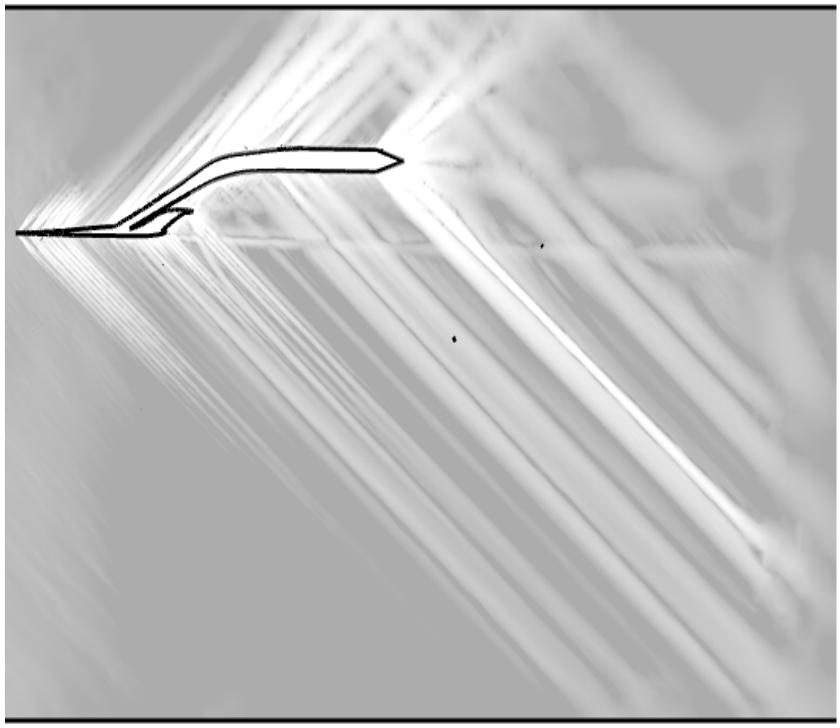

(b) USM3D simulation for LBC in Tunnel.

(c) AERO simulation for LBC in Tunnel.

Figure 34. Concluded.